





ORIGINAL RESEARCH

 OPEN ACCESS 

Interleukin-1 β provided by KIT-competent mast cells is required for *KRAS*-mutant lung adenocarcinoma

Ioannis Lilis^a, Giannoula Ntaliarda^a, Vassilios Papaleonidopoulos ^a, Georgia A Giotopoulou^a, Maria Oploupoiou^a, Antonia Marazioti^a, Magda Spella^a, Sebastian Marwitz^b, Torsten Goldmann^b, Vasiliki Bravou^c, Ioanna Giopanou ^a, and Georgios T. Stathopoulos ^{a,d}

^aLaboratory for Molecular Respiratory Carcinogenesis, Department of Physiology, Faculty of Medicine, University of Patras, Rio, Achaia, Greece; ^bClinical and Experimental Pathology, Research Center Borstel, Airway Research Center North (ARCN), Member of the German Center for Lung Research (DZL), Borstel, Germany; ^cDepartment of Anatomy-Histology-Embryology, Faculty of Medicine, University of Patras, Rio, Achaia, Greece; ^dComprehensive Pneumology Center (CPC) and Institute for Lung Biology and Disease (ILBD), University Hospital, Ludwig-Maximilians University and Helmholtz Zentrum München, Member of the German Center for Lung Research (DZL), Munich, Bavaria, Germany

ABSTRACT

Mast cells (MC) have been identified in human lung adenocarcinoma (LADC) tissues, but their functional role has not been investigated *in vivo*. For this, we applied three mouse models of *KRAS*-mutant LADC to two different MC-deficient mouse strains (*cKit^{Wsh}* and *Cpa3.Cre*). Moreover, we derived MC gene signatures from murine bone marrow-derived MC and used them to interrogate five human cohorts of LADC patients. Tumor-free *cKit^{Wsh}* and *Cpa3.Cre* mice were deficient in alveolar and skin KIT-dependent (KIT+) MC, but *cKit^{Wsh}* mice retained normal KIT-independent (KIT-) MC in the airways. Both KIT+ and KIT- MC infiltrated murine LADC to varying degrees, but KIT+ MC were more abundant and promoted LADC initiation and progression through interleukin-1 β secretion. KIT+ MC and their transcriptional signature were significantly enriched in human LADC compared to adjacent normal tissue, especially in the subset of patients with *KRAS* mutations. Importantly, MC density increased with tumor stage and high overall expression of the KIT+ MC signature portended poor survival. Collectively, our results indicate that KIT+ MC foster LADC development and represent marked therapeutic targets.

ARTICLE HISTORY

Received 1 August 2018
Revised 23 February 2019
Accepted 28 February 2019

KEYWORDS

Carboxypeptidase
3/mutation/IL; 1 β /lung
cancer/urethane

Introduction

Lung adenocarcinoma (LADC) is the number one cancer killer worldwide, constituting the majority of newly diagnosed lung cancer cases and continuously rising in incidence.^{1,2} Epidemiologic and molecular evidence indicates an increased risk of LADC harboring mutations in the *KRAS* proto-oncogene GTPase (*KRAS*) in ever-smoking individuals.^{1,3} These patients also feature smoking-associated chronic inflammation that is clinically evident as chronic airflow obstruction.^{4–7} It is generally believed that this inflammation alters the microenvironment of tobacco carcinogen-mutated respiratory epithelial cells, fostering their survival and sustained growth instead of their eradication.^{4,8} This pulmonary inflamed microenvironment of smokers encompasses complex interactions between tumor-initiated respiratory epithelial cells and host immune cells and has been only poorly charted.^{9–11}

Mast cells (MC) are bone marrow-derived inflammatory leukocytes which can secrete upon activation a battery of biologically active products.^{12–15} MC are distributed in all vascularized tissues and are particularly abundant at the bodily interfaces to the environment, including the lungs, skin, and gut.^{14,16–19}

Although MC are well-recognized initiators of acute allergic reactions, it is now apparent that these multifarious cells infiltrate a wide spectrum of malignancies and execute various important functions in tumor initiation and progression.^{20–24} To this end, MC play pro-tumorigenic roles in some malignancies (i.e., gastric, prostate, and pancreatic cancers), gate-keeper roles in others (i.e., breast and ovarian cancers), and function as innocent bystanders in yet others.²⁵ While the reasons for divergent MC functions in cancer remain elusive, new models of MC ablation lend promise to solve this riddle but have not been widely employed in cancer models.^{26,27}

MC have been identified in human and murine LADC, and have been found to promote lung adenocarcinoma cell growth *in vitro* and to be associated with poor patient survival.^{28–31} We recently showed that *KRAS* mutations in tumor cells and host co-opted MC cooperate to promote the development of an inflammatory chemokine signaling network that culminates in metastatic malignant pleural effusions.^{32–34} However, the functional role of MC in *KRAS*-mutant LADC development remained elusive. Here we generated various types of *KRAS*-mutant LADC in two different mouse models of MC ablation (*cKit^{Wsh}* and *Cpa3.Cre* mice) that feature, respectively, selective

CONTACT Georgios T. Stathopoulos  gstathop@upatras.gr; Ioannis Lilis  ioannislilis@upatras.gr  Biomedical Sciences Research Building, 2nd floor, Room B40; 1 Asklepiou Str., University Campus, Rio 26504, Greece
Ioannis Lilis and Giannoula Ntaliarda are equally contributing first authors
Georgios T. Stathopoulos and Ioanna Giopanou are equally contributing senior authors

© 2019 The Author(s). Published with license by Taylor & Francis Group, LLC.

This is an Open Access article distributed under the terms of the Creative Commons Attribution-NonCommercial-NoDerivatives License (<http://creativecommons.org/licenses/by-nc-nd/4.0/>), which permits non-commercial re-use, distribution, and reproduction in any medium, provided the original work is properly cited, and is not altered, transformed, or built upon in any way.

elimination of KIT-dependent MC and complete ablation of all MC. Interestingly, KIT-dependent MC were more abundant and were found to promote experimental *KRAS*-mutant LADC initiated by the tobacco carcinogen urethane, by oncogenic *KRAS*^{G12D} expression in the lungs, and by transplanted LADC cells. KIT-dependent MC and their transcriptome signatures were evident in different human LADC cohorts and correlated with poor survival, indicating a potential actionable role for these cells in human disease progression.

Results

Mast cells infiltrate murine lung adenocarcinomas

To identify whether MC infiltrate experimental LADC, we used three different mouse models of the disease arising in distinct anatomical compartments. In a first line of experiments, *C57BL/6* mice received 10 consecutive weekly intraperitoneal injections of the tobacco-contained carcinogen urethane (1g/Kg) and were sacrificed after six months, a model that results in stochastic chemical mutagenesis of the airway epithelium (Figure 1A, D).^{35–38} Alternatively, *C57BL/6* mice carrying a conditional loxP-STOP-loxP. *KRAS*^{G12D} allele (*KRAS*^{G12D} mice) received 5×10^8 intratracheal plaque-forming units (pfu) Ad-*Cre* and were killed after four months. In this model, progressive lesions carrying the inciting *KRAS*^{G12D} mutation are inflicted in alveolar epithelial cells infected by Ad-*Cre* via excision of the STOP codon that hinders expression of the mutant transgene (Figures 1B, E).^{39,40} In a third line of experiments, *C57BL/6* mice received 10^6 LLC cells into the rear flank dermis, a model of established LADC heterotopic growth and spontaneous pulmonary metastasis (Figures 1C, F).^{41–43} We labeled with the metachromatic stain toluidine blue (TB) that distinctively stains MC violet on a blue background and systematically evaluated MC abundance on randomly sampled sections of lungs from the former two models, and primary tumors and lungs with metastases from the latter model, as well as tumor-free lungs of *C57BL/6* mice ($n = 10$ /group). MC were identified in LADC of all three models examined, preferentially located in early lesions, at the tumor front, at subbronchial and subpleural sites, or within alveolar inflammatory infiltrates frequently observed in juxtatumoral areas (Figures 1G–N). Importantly, alveoli were less MC-dense, and MC infiltrates of urethane-induced tumors were less prominent compared with the *KRAS*^{G12D} and LLC models (Figure 1O). Overall, MC infiltrates accounted for approximately 1 in 50 tumor cells. These findings are in accord with a previous report from the urethane model,²⁹ and indicate that MC are present in experimental LADC developing in the airways, alveoli, and skin.

Compartmentalized mast cell deficiency of *cKit*^{Wsh} and *Cpa3.cre* mice

We next assessed lung and skin MC density in two different strains of genetically MC-deficient mice that either lack functional KIT receptors required for mastopoiesis (*cKit*^{Wsh} mice),^{33,44} or express CRE recombinase exclusively in MC leading to tumor-related protein 53 (TRP53)-mediated spontaneous

apoptosis of these cells (*Cpa3.Cre* mice).^{27,33} For this, the airways, alveoli, and skin of mice on a pure *C57BL/6* background carrying one or two *cKit*^{Wsh} alleles (designated *cKit*^{Wsh/Wt} and *cKit*^{Wsh/Wsh}, respectively) or one *Cpa3.Cre* allele, as well as littermate controls of both strains (collectively designated *C57BL/6*; $n = 10$ /group; total $n = 40$) were sectioned and stained with toluidine blue. In more detail, the control *C57BL/6* group consisted of *cKit*^{Wt/Wt} littermates of *cKit*^{Wsh/Wt} and *cKit*^{Wsh/Wt} mice, wild-type (*Wt*) littermates of *Cpa3.Cre* mice, as well as *Lyz2.Cre* mice that express CRE recombinase under the control of the endogenous *Lyz2* promoter as additional controls for *Cpa3.Cre* mice.⁴⁵ Surprisingly, MC were identified throughout the airways of *C57BL/6*, but also of *cKit*^{Wsh/Wt} and *cKit*^{Wsh/Wsh} mice and were absent from the airways of *Cpa3.Cre* mice. In contrast, MC were present in the alveolar regions, pulmonary vasculature, mediastinal organs, and the skin of *C57BL/6* mice, but were significantly decreased in these compartments of *cKit*^{Wsh/Wt}, *cKit*^{Wsh/Wsh}, and *Cpa3.Cre* mice (Figures 2A–G). These results are consistent with the initial descriptions of these mice,^{27,44} as well as with our previous study of pleural MC,³³ and indicate that *cKit*^{Wsh/Wsh} and *Cpa3.Cre* mice can serve as compartmentalized mouse models of MC deficiency of the alveoli/skin and of the airways/alveoli/skin, respectively (Figure 2H).

Mast cells are required for lung adenocarcinoma formation and progression

To determine whether MC are functionally involved in LADC development, we reproduced all three mouse models of airway, alveolar, and cutaneous LADC described above in *C57BL/6* (*Wt* littermates and *Lyz2.Cre* heterozygotes), *cKit*^{Wsh/Wt}, *cKit*^{Wsh/Wsh}, and *Cpa3.Cre* mice. In a first line of experiments, *C57BL/6*, *cKit*^{Wsh/Wt}, *cKit*^{Wsh/Wsh}, and *Cpa3.Cre* mice received 10 consecutive weekly intraperitoneal urethane (1g/Kg) injections (total $n = 143$; Figure 3A). Thirty-eight mice succumbed to repeat carcinogen treatment (14 of 58 *C57BL/6*, 2 of 21 *cKit*^{Wsh/Wt}, 21 of 55 *cKit*^{Wsh/Wsh}, and 1 of 9 *Cpa3.Cre* mice; $\chi^2 P = 0.0419$, Fisher's exact $P = 0.0236$ for comparison of *cKit*^{Wsh/Wt} with *cKit*^{Wsh/Wsh} mice), while the remaining 105 mice were sacrificed after six months for lung tumor evaluation (Figure 3B). *Cpa3.Cre* mice were markedly protected from urethane-induced bronchial carcinomas in terms of tumor multiplicity, size, and cellular proliferation rate, suggesting an important role for MC in tumor initiation and progression, whereas *cKit*^{Wsh/Wt} and *cKit*^{Wsh/Wsh} mice were susceptible to the carcinogen to a degree similar to *C57BL/6* mice, a result consistent with their sufficiency in MC of the airways, the site of tumor initiation induced by urethane (Figure 3C–E). In a second line of experiments, *KRAS*^{G12D} *KRAS*^{G12D} *cKit*^{Wsh/Wt}, and *KRAS*^{G12D} *cKit*^{Wsh/Wsh} mice (*C57BL/6* background) received 5×10^8 intratracheal pfu Ad-*Cre* and were killed after four months. *KRAS*^{G12D} \times *Cpa3.Cre* intercrosses failed to generate double heterozygote offspring suggesting fetal lethality ($n =$ three intercrosses; 11 litters; 53 off-springs; $P = 0.0001$ for 0/53 genotype frequencies obtained compared to 13/40 expected by Fischer's exact test). *KRAS*^{G12D} *cKit*^{Wsh/Wsh} mice were significantly protected from *KRAS*-driven alveolar carcinomas compared with *KRAS*^{G12D} mice, with *KRAS*^{G12D} *cKit*^{Wsh/Wt} mice

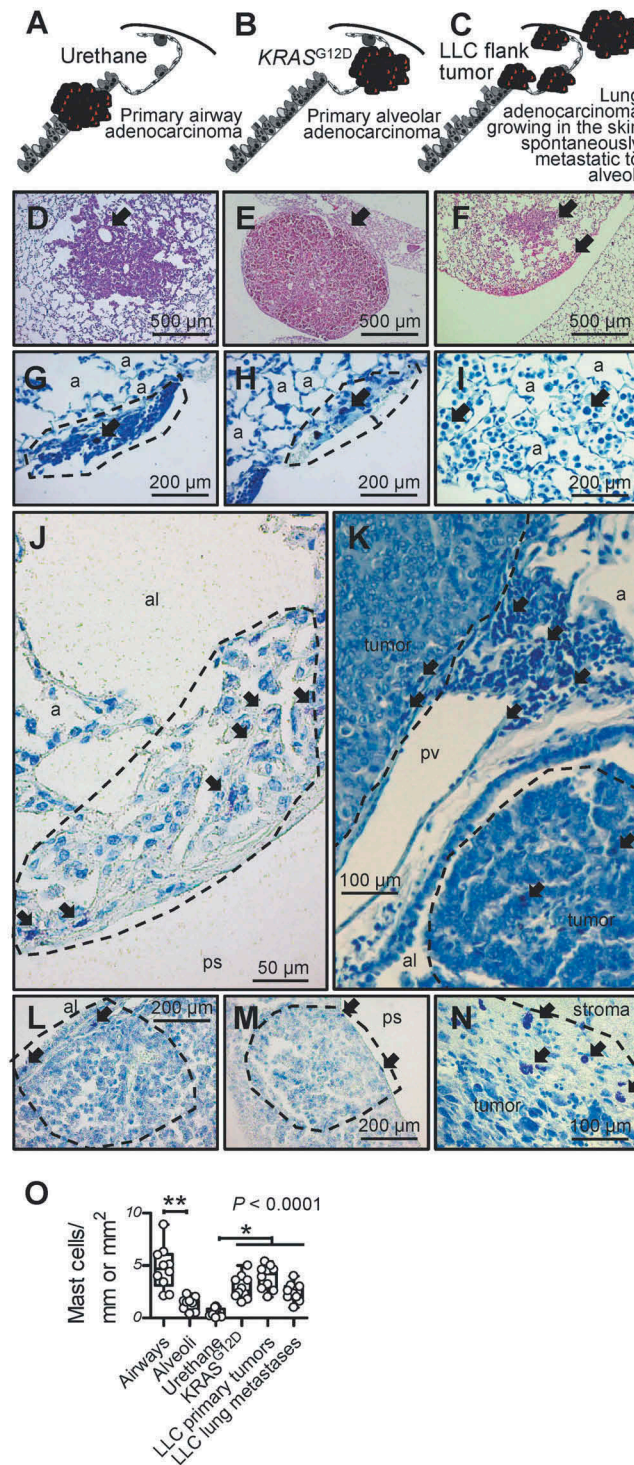


Figure 1. Mast cells in murine lung adenocarcinomas.

A-F Schematics depicting tumors (red) of the airways, alveoli, and skin (A-C) and representative microscopic images of hematoxylin/eosin-stained sections (D-F) of airway-originated lung adenocarcinomas (LADC) induced in *C57BL/6* mice by 10 weekly consecutive intraperitoneal injections of 1 g/Kg urethane (six months latency; A and D; arrow in D denotes originating bronchus), of alveolar-derived LADC induced in *KRAS^{G12D}*-transgenic mice by intratracheal injection of 5×10^8 pfu Ad-Cre (four months latency; B and E; arrow in E denotes originating alveolar region), and of skin heterotopic LADC spontaneously metastasizing to the alveolar regions induced by subcutaneous delivery of 10^6 LLC cells (one month latency; C and F; arrows in F denote alveolar regions involved by metastases). G-N Toluidine blue-stained lung and tumor sections from the above-described three mouse models of LADC showing metachromatic (purple) mast cells (arrows) in early urethane-induced atypical alveolar hyperplasias (dashed lines in G and H), in tumor-adjacent alveolar inflammatory infiltrates (I), in and adjacent to urethane-induced LADC (dashed lines in J and K), entering alveolar *KRAS^{G12D}*-transgenic tumors from the airway lumen and the pleural space (dashed lines, L and M), and in subcutaneous LLC tumor (dashed line in N). a, alveoli; al, airway lumen; ps, pleural space; pv, pulmonary vein. O Mast cell abundance of urethane- and *KRAS^{G12D}*-primary tumors and LLC primary tumors and metastases compared with airways and alveoli of naïve *C57BL/6* mice ($n = 10$ /group). Data are presented as median with Tukey's whiskers (boxes: interquartile range; bars: 50% extreme quartiles), raw data points (dots), and Kruskal-Wallis analysis of variance (ANOVA) probability (P) value.* and **: $P < 0.05$ and $P < 0.01$, respectively, for the indicated comparisons by Dunn's post-tests. Only statistically significant differences are indicated.

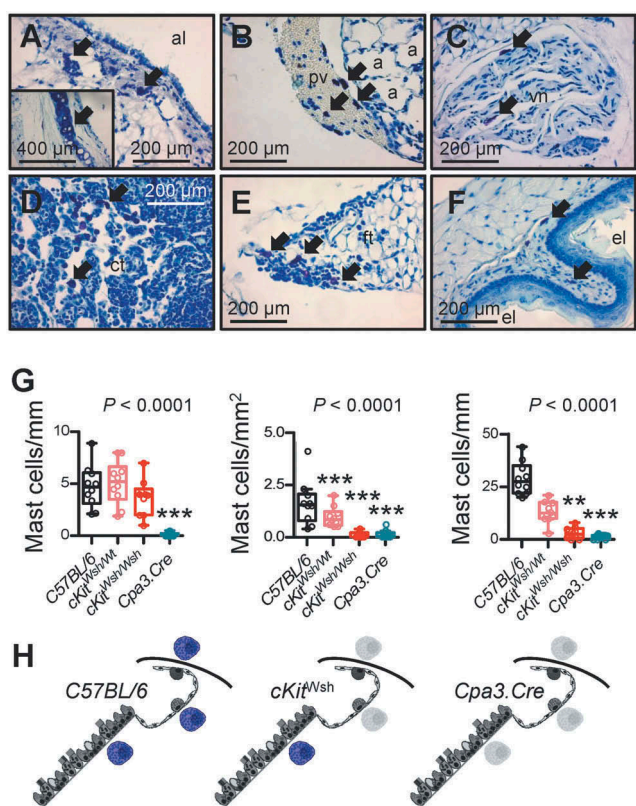


Figure 2. Thoracic and skin mast cells in two different mouse models of mast cell deficiency.

The airways, alveoli, and skin of mice carrying one or two *cKit^{Wsh}* alleles (designated *cKit^{Wsh/Wt}* and *cKit^{Wsh/Wsh}*, respectively) or one *Cpa3.Cre* allele on a pure *C57BL/6* background, and *C57BL/6* littermate or *Lyz2.Cre* heterozygous control mice ($n = 10/\text{group}$) were sectioned and stained with toluidine blue. Representative microscopic images of toluidine blue-stained tissue sections (A–F), summary of data from $n = 10$ mice/group (G), and schematics of mast cell competence (colored mast cells) and deficiency (grey mast cell shadows) (H). A–F Arrows indicate mast cells in the submucosa of a large airway (A; inlay shows tracheal cartilage as positive control of metachromatic purple staining), in a large pulmonary vein (B), in the vagus nerve (C), in the thymus of a 6-week-old (D) and a 20-week-old (E) mouse, and in the esophageal submucosa (F) of *C57BL/6* controls. a, alveoli; pv, pulmonary vein; al, airway lumen; vn, vagus nerve; ct, cellular thymus; ft, fatty thymus; el, esophagus lumen. G Airway, alveolar, and skin mast cell density of *C57BL/6* control, *cKit^{Wsh/Wt}*, *cKit^{Wsh/Wsh}*, and *Cpa3.Cre* mice (summary of data from $n = 10$ mice/group). Shown are median with Tukey's whiskers (boxes: interquartile range; bars: 50% extreme quartiles), raw data points (dots), and Kruskal–Wallis analysis of variance (ANOVA) probability (P) value. **, and ***: $P < 0.01$ and $P < 0.001$, respectively, for comparisons with *C57BL/6* controls by Dunn's post-tests. Only statistically significant differences are indicated. Note the airway mast cell competence of *cKit^{Wsh/Wt}* and *cKit^{Wsh/Wsh}* mice, and the complete mast cell deficiency of *Cpa3.Cre* mice. H Schematics depicting mast cells (purple) of the airways, alveoli, and skin of *C57BL/6*, *cKit^{Wsh/Wt}*, *cKit^{Wsh/Wsh}*, and *Cpa3.Cre* mice. Grey mast cell fade-outs indicate mast cell deficiency of the given anatomic compartment.

displaying an intermediate phenotype, indicating a significant tumor-promoting role of MC in the disease (Figure 4). Finally, separate cohorts of *C57BL/6*, *cKit^{Wsh/Wt}*, *cKit^{Wsh/Wsh}*, and *Cpa3.Cre* mice, all on the *C57BL/6* background, received 10^6 subcutaneous LLC cells and were followed for one month. *cKit^{Wsh/Wsh}* and *Cpa3.Cre* mice displayed significantly delayed primary tumor growth, as well as decreased spontaneous metastasis to the lungs compared with controls; interestingly, *cKit^{Wsh/Wt}* mice displayed sustained primary tumor growth, but significantly decreased metastasis (Figure 5A–C). Co-labeling of MC and proliferating cells in primary tumors from these mice using

toluidine blue and anti-proliferating cell nuclear antigen (PCNA) antibody revealed that MC directly contacted PCNA+ tumor cells (Figures 5D–J), that LLC tumors of *Cpa3.Cre* mice had decreased numbers of proliferating tumor cells and were devoid of MC, while *cKit^{Wsh/Wt}* and *cKit^{Wsh/Wsh}* mice displayed intermediate phenotypes, and that PCNA+ tumor cells were significantly increased in MC hotspots of LLC tumors of control mice (Figures 5K–N). Collectively, these data indicate that MC are important for LADC development, growth, and metastasis.

Mast cells respond to lung adenocarcinoma-secreted factors

To identify MC-derived mediators that drive LADC, we isolated MC from *C57BL/6* mouse bone marrow (bone marrow-derived MC, BMMC) using one month's incubation with 100 ng/mL interleukin (IL)-3 alone or 100 ng/mL IL-3 plus 100 ng/mL KIT ligand (KITL), a method that yields > 95% pure BMMC, as described elsewhere.³³ KIT-dependent (KIT+) and KIT-independent (KIT-) BMMC were then exposed to cell-free LLC-conditioned media (CM) for 24 h and their RNA was examined for changes in gene expression compared with non-CM-exposed counterparts by microarray [Gene Expression Omnibus (GEO) identifier GSE58189; <https://www.ncbi.nlm.nih.gov/geo/query/acc.cgi?acc=GSE58189>]. This experiment revealed distinct gene sets that are differentially regulated in KIT+ and KIT- BMMC or both upon LADC cell encounter (Figure 6A, B). The human orthologues of the top transcripts of these three sets were used to compile KIT+, KIT-, and common MC signatures and included *Il1b* (Figure 6C), which we previously identified to promote LADC-induced malignant pleural effusion.³³ *Ex-vivo* generated KIT+ BMMC displayed marked increases in IL-1 β production and caspase-1 (CASP1) expression upon LADC cell encounter (Figure 6D–F), consistent with the role of CASP1 in IL-1 β processing.⁴⁶ IL-1 β also promoted subcutaneous LADC growth, since *Il1b*-deficient mice displayed significantly delayed tumor growth after subcutaneous LLC injection (Figure 6H). These results indicate that both KIT+ and KIT- MC respond transcriptionally to LADC-secreted factors and identify candidate gene sets of MC-derived LADC promoters for future research. In addition, the data support that MC can develop and respond to tumor cells in the absence of functional KIT (i.e., in *cKit^{Wsh/Wt}* and *cKit^{Wsh/Wsh}* mice).

Mast cells impact the microenvironment of lung adenocarcinoma

We next evaluated the abundance of other immune cells in our experimental LADC models on backgrounds of MC-competence and -deficiency. While mononuclear and lymphoid cells were equally abundant in LADC from MC-competent and -deficient mice, we observed a statistically significant increase in polymorphonuclear cells in *cKit^{Wsh/Wsh}* mice (Figure 7A–F), in accord with a previous report.⁴⁷ Interleukin-1 β immunoreactivity was statistically significantly decreased in LADC from MC-deficient mice, indicating that MC are a cardinal source of the cytokine in LADC (Figure 7G). We next co-labeled MC with anti-KIT antibody and toluidine blue in LADC of MC-competent mice, to observe that KIT+ MC were more abundant compared with

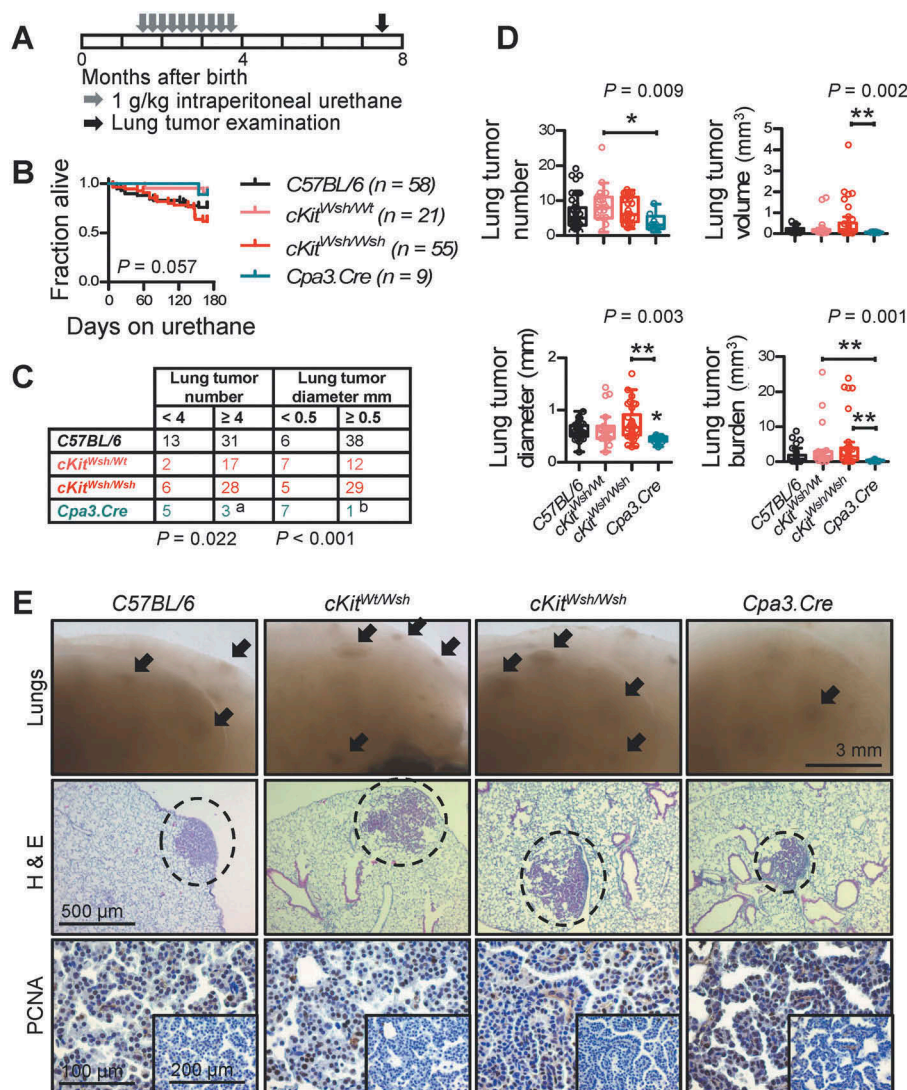


Figure 3. Mast cell deficiency protects mice from urethane-induced lung adenocarcinoma of the airways.

$C57BL/6$ controls ($cKit^{Wt/Wt}$ and $Cpa3.Cre^{-/-}$ littermate controls, as well as $Lyz2.Cre$ mice), $cKit^{Wsh/Wt}$, $cKit^{Wsh/Wsh}$, and $Cpa3.Cre$ mice received ten consecutive weekly intraperitoneal urethane (1g/Kg) injections ($n = 58, 21, 55,$ and $9,$ respectively) and were followed for survival and lung tumor analyses at six months post-urethane start. **A** Schematic time-course of the experiment with boxes representing one month. **B** Kaplan–Meier survival curves and log-rank P value. **C** Frequency distribution of tumor number and size with n and χ^2 P values. **a:** $P < 0.05$ for $Cpa3.Cre$ mice compared with $cKit^{Wsh/Wt}$ and $cKit^{Wsh/Wsh}$ mice by Fischer's exact test. **b:** $P < 0.05$ for $Cpa3.Cre$ mice compared with $cKit^{Wsh/Wt}$ mice and $P < 0.001$ for $Cpa3.Cre$ mice compared with $C57BL/6$ control and $cKit^{Wsh/Wsh}$ mice by Fischer's exact test. **D** Data summary of tumor number, size, mean volume, and burden per lung shown as median with Tukey's whiskers (boxes: interquartile range; bars: 50% extreme quartiles), raw data points (dots), and Kruskal–Wallis analysis of variance (ANOVA) probability (P) value. *, and **: $P < 0.05$, and $P < 0.01$, respectively, for the indicated comparisons by Dunn's post-tests. Only statistically significant differences are indicated. **E** Representative images of gross lungs and hematoxylin/eosin (H&E)- and proliferating cell nuclear antigen (PCNA)-stained lung sections. Arrows and dashed lines denote lung adenocarcinomas.

KIT- MC (Figure 7H, I). Collectively, these findings indicate that KIT+ MC are the predominant MC population in LADC that regulate the recruitment of other immune cells and that contribute to IL-1 β secretion.

Interleukin-1 β provided by KIT+ mast cells is required for KRAS-mutant LADC

Based on the *in vivo* results obtained from the different mouse models of LADC, we hypothesized that KIT+ and KIT- MC may possess different LADC-promoting properties. To test this, as well as to determine the impact of IL-1 β on LADC growth, BMMC were cultured from *WT* and *Il1b*^{-/-} mice,⁴⁸ as described above and elsewhere.³³ After 30 days in culture on 100 ng/mL

IL-3 alone or 100 ng/mL IL-3 plus 100 ng/mL KITL, more than 95% of BMMC from both *WT* and *Il1b*^{-/-} mice differentiated into MC of various maturation stages displaying metachromasia, i.e. purple staining with toluidine blue (Figure 8A), as well as MC-specific molecular markers. We next co-cultured LLC cells with DMEM control or with KIT+ or KIT- BMMC from *WT* or *Il1b*^{-/-} mice at a physiologically relevant 50:1 ratio identified from *in vivo* LADC (Figures 10, 8A). Co-cultures were assessed for *in vitro* cellular proliferation by 3-(4,5-dimethylthiazol-2-yl)-2,5-diphenyltetrazolium bromide (MTT) reduction, for *in vitro* cell migration by scratch assay, and for *in vivo* tumor growth after subcutaneous injection of a million cells into syngeneic *Ccr2* gene-deficient mice ($n = 5$ –6/group), selected to prevent confounding chemorecruitment of endogenous host mouse

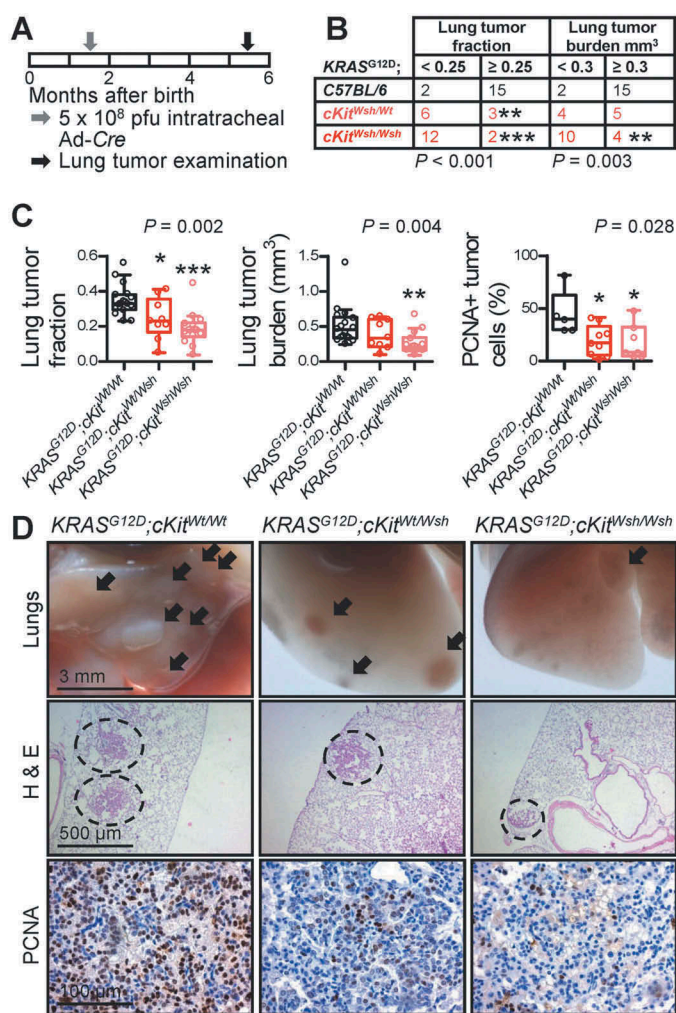


Figure 4. Mast cell deficiency protects mice from *KRAS*^{G12D}-induced lung adenocarcinoma of the alveoli.

KRAS^{G12D} *KRAS*^{G12D} *cKit*^{Wsh/Wt}, and *KRAS*^{G12D} *cKit*^{Wsh/Wsh} mice (*C57BL/6* background) received 5 × 10⁸ intratracheal plaque-forming units (pfu) Ad-Cre and were killed after four months (*n* = 17, 9, and 14, respectively). A Schematic time-course of the experiment with boxes representing one month. B Frequency distribution of relative lung tumor fraction and absolute lung tumor volume (burden) with *n* and χ^2 *P* values. ** and ***: *P* < 0.01 and *P* < 0.001, respectively, for comparisons with *KRAS*^{G12D} controls by Fischer's exact test. C Data summary of relative lung tumor fraction and absolute lung tumor volume (burden) per lung, as well as percentage of proliferating cell nuclear antigen (PCNA)+ tumor cells with Tukey's whiskers (boxes: interquartile range; bars: 50% extreme quartiles), raw data points (dots), and Kruskal–Wallis ANOVA *P* values. *, **, and ***: *P* < 0.05, *P* < 0.01, and *P* < 0.001, respectively, for comparison with *KRAS*^{G12D} controls by Dunn's post-tests. Only statistically significant differences are indicated. D Representative images of gross lungs and hematoxylin/eosin (H & E)- and PCNA-stained lung sections. Arrows and dashed lines denote lung adenocarcinomas.

MC.^{33,49} These experiments clearly showed that exclusively KIT+ MC competent in IL-1 β can promote LADC cell proliferation and migration *in vitro* and *in vivo* (Figure 8B–D).

Mast cells in human lung adenocarcinoma

To determine whether our findings are relevant to human LADC, we analyzed MC infiltrates in 37 patients with histologically documented LADC from one of our previous studies from

Greece.⁵⁰ MC preferentially accumulated in tumor tissue compared with adjacent normal-appearing lung tissue (Figure 9A; Table 1). In addition, the human orthologue of the murine KIT+ MC signature above, generated at <http://lighthouse.ucsf.edu/orthoretriever/>,⁵¹ was significantly over-represented in tumor tissue compared with adjacent lung tissues of 10 patients with histologically documented LADC from one of our previous studies from Germany (Figure 9B; Table 2).⁵² Individual transcripts from all three MC signatures, including *TNFRSF9* and *CD72* from the common, *NLRP6* from the KIT-, as well as *SLC43A3*, *TRAF1*, and *HSPA1B* from the KIT+ MC signature were significantly over-represented in tumor tissue compared with adjacent lung tissue (Figure 9C). In addition, MC density significantly increased with T, N, and TNM stage in the former series of patients (Figure 9D–I). These results are in line with the increased tumor cell proliferation indices of LADC from MC-competent mice compared with MC-deficient counterparts and suggest that MC infiltrate human LADC, where they exert pro-tumor functions. Moreover, the data suggest that primarily KIT+ MC infiltrate human LADC. We further interrogated the presence of MC transcriptional signatures in human LADC, employing published transcriptomes of normal lung tissues from never smokers and LADC tissues from never- and current smokers from the Biomarker-integrated Approaches of Targeted Therapy for Lung Cancer Elimination (BATTLE) study (GEO dataset GSE43458; <https://www.ncbi.nlm.nih.gov/geo/query/acc.cgi?acc=GSE43458>).⁵³ Unsupervised clustering of this patient cohort by our humanized transcriptional signatures of KIT+ and KIT- MC accurately discriminated normal from LADC tissues and several genes of these MC signatures were overrepresented in tumor versus normal tissues, but also in smokers' versus never-smokers' LADC, validating the results from our small cohort from Germany (Figure 10A, B).⁵² Although all MC signatures could discern LADC tissues from normal lungs, the KIT+ signature emerges to be functionally important in LADC, since LADC patients with high expression of exclusively this footprint displayed significantly shorter survival (<http://kmplot.com/analysis/index.php?p=service&cancer=lung>; Figure 10C).⁵⁴ Finally, gene set enrichment analyses (GSEA) of humanized KIT+ and KIT- MC signatures were done in LADC from smokers and never smokers compared with normal lung tissue (GEO dataset GSE43458; <https://www.ncbi.nlm.nih.gov/geo/query/acc.cgi?acc=GSE43458>) and in *KRAS*- and *EGFR*-mutant LADC compared with normal lung tissue (GEO dataset GSE31852; <https://www.ncbi.nlm.nih.gov/geo/query/acc.cgi?acc=GSE31852>).^{53,55,56} Using stringent cut-offs of false discovery rate (FDR) *q* values < 0.05 and family-wise error rate (FWER) probability (*P*) values < 0.05, we found that exclusively the KIT+ MC signature was focally enriched in *KRAS*-mutant LADC, while missing significance levels by a margin in smokers' LADC (Figure 11). These results connect KIT+ MC with *KRAS*-mutant LADC caused by tobacco smoking, in line with the results from the animal models of *KRAS*-mutant LADC employed (Figures 1–5). Collectively, these results from five human cohorts of LADC indicated that both KIT+ and KIT- MC and their transcriptional signatures are present in human LADC, and suggested that KIT+ MC are specifically important for disease progression of *KRAS*-mutant LADC.

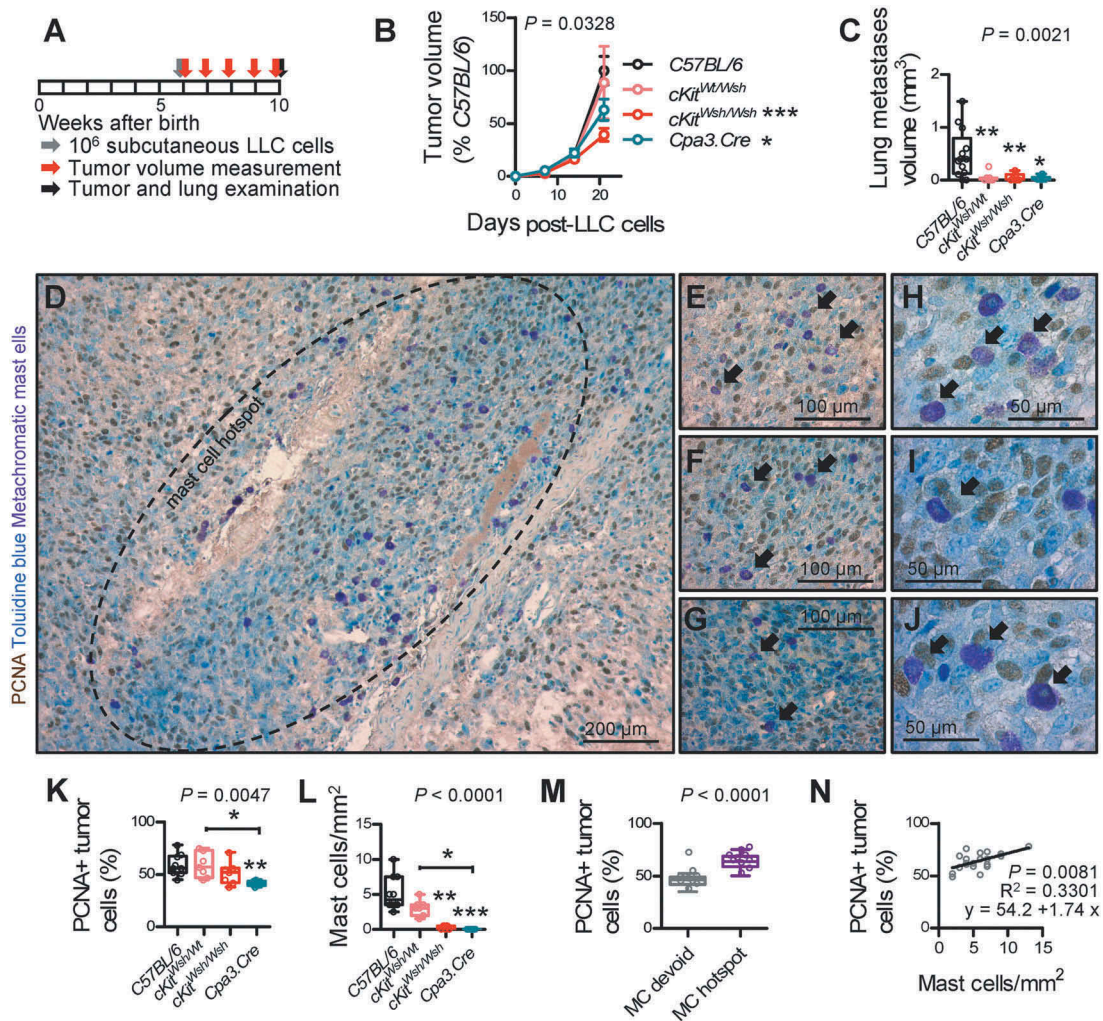


Figure 5. Mast cell deficiency protects mice from Lewis lung adenocarcinoma growth in the skin and its metastasis to the alveolar regions.

C57BL/6 controls (*cKit*^{Wt/Wt} and *Cpa3.Cre*^{-/-} littermate controls, as well as *Lyz2.Cre* mice), *cKit*^{Wsh/Wt}, *cKit*^{Wsh/Wsh}, and *Cpa3.Cre* mice, all on the *C57BL/6* background ($n = 13, 7, 7,$ and $6,$ respectively), received 10^6 subcutaneous Lewis lung carcinoma cells (LLC), were followed for one month by weekly measurement of three vertical primary tumor diameters (δ) and calculation of primary flank tumor volume ($V = \pi\delta^3/6$) and were sacrificed for primary tumor and spontaneous lung metastasis analyses at one month post-LLC cells. A Schematic time-course of the experiment with boxes representing one week. B Data summary of primary subcutaneous tumor volume expressed as percentage of *C57BL/6* controls (mean \pm SEM) with two-way ANOVA P value. * and ***: $P < 0.05$ and $P < 0.001$, respectively, for comparison with *C57BL/6* controls by Bonferroni post-tests. C Data summary of absolute lung metastasis volume (burden) per lung. D–J Toluidine blue-counterstained primary LLC tumor sections of *C57BL/6* control mice ($n = 10$) labeled for proliferating cell nuclear antigen (PCNA), a technique that allows simultaneous visualization and quantification of proliferating cells (brown), mast cells (purple), and nuclei (blue). Shown are representative mast cell hotspot (D; dashed line) and areas of such hotspots featuring mast cells in close association/contact with proliferating tumor cells (E–J; arrows). K–N Data summary of percentage of PCNA+ primary tumor cells (K), primary tumor mast cell density (L), percentage of PCNA+ cells in mast cell hotspots versus mast cell-devoid areas of primary tumors of *C57BL/6* mice (M), and correlation of these two parameters in mast cell hotspots of primary tumors of *C57BL/6* mice (N). (K, L) $n = 10, 7, 7,$ and $6,$ respectively. (M) $n = 10$ *C57BL/6* mice. (N) $n = 2$ hotspots from each of 10 *C57BL/6* mice. Data information: (C, K, L, M) Data are shown as Tukey's whiskers (boxes: interquartile range; bars: 50% extreme quartiles), raw data points (dots), and Kruskal–Wallis ANOVA (C, K, L) and Mann–Whitney u -test (M) P values. *, **, and ***: $P < 0.05$, $P < 0.01$, and $P < 0.001$, respectively, for comparison with *C57BL/6* controls or as indicated by Dunn's post-tests. Only statistically significant differences are indicated. (N) Shown are data points, Pearson correlation P value and coefficient, and linear regression line and formula.

Discussion

This is the first *in vivo* study on the role of mast cells in lung adenocarcinoma. We show that KIT+ MC possess potent biological activity fostering disease progression in three different mouse models of KRAS-mutant LADC either endogenously arising from the airways or the alveoli, or heterotopically implanted in the skin and spontaneously disseminating to the alveolar areas. For this, we used two divergent genetic models of MC deficiency, one resting on defective KIT signaling (*cKit*^{Wsh} mice) and another relying on genetic MC ablation (*Cpa3.Cre* mice). The results indicate that KIT+ MC are required for

LADC, since each MC-deficient strain was markedly protected from tumorigenesis in at least two models of LADC: *cKit*^{Wsh} mice from KRAS^{G12D}- and LLC-induced tumors, and *Cpa3.Cre* mice from urethane and LLC-induced tumors. Albeit both MC populations infiltrate experimental and human LADC, we show how KIT+ MC foster LADC progression conditional on their competence for IL-1 β secretion, while KIT- MC appear to have a neutral role. Moreover, we identify MC gene sets that are differentially regulated upon LADC cell encounter, facilitating the future discovery of MC-derived effectors that foster LADC. Human results from five different patient cohorts lend support to our experimental findings of an LADC promoting role for

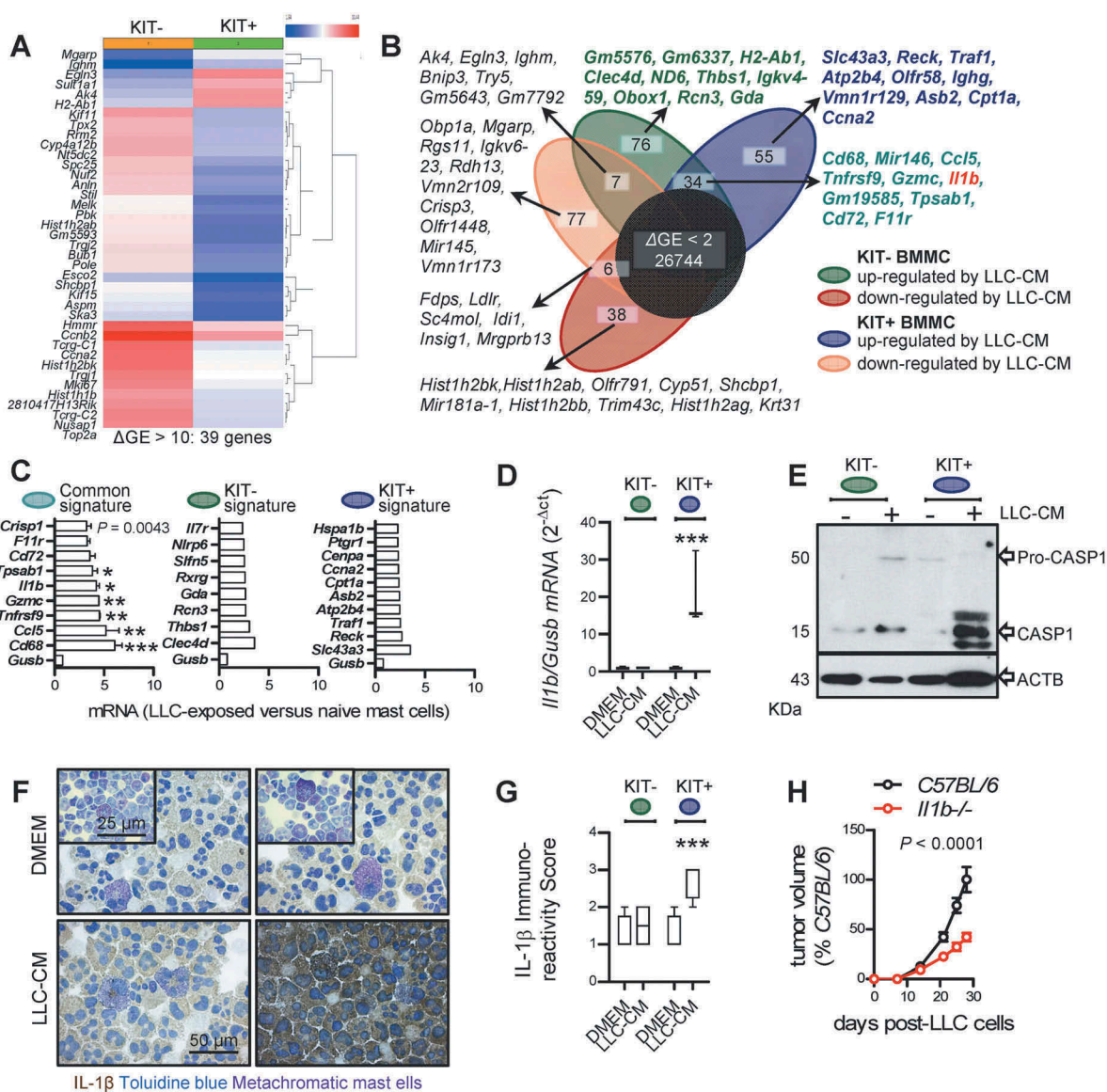


Figure 6. Response of bone marrow-derived mast cells to lung adenocarcinoma cells and lung adenocarcinoma growth in interleukin-1 β -deficient mice.

A Genes differentially expressed (39 genes, $\Delta GE \geq 2$) between KIT-dependent (KIT+) and KIT-independent (KIT-) bone marrow-derived mast cells (BMMC). B Venn diagram of differentially expressed genes ($\Delta GE \geq 2$) of BMMC pre-cultured for one month with interleukin (IL-3) plus cKIT ligand (KIT+ BMMC) or with IL-3 only (KIT- BMMC) upon 24-h incubation with cell-free Lewis lung carcinoma-conditioned media (LLC-CM) by Affymetrix Mouse Gene ST2.0 microarrays. Top 10 transcripts from each gene set are listed. Note the 55 genes selectively up-regulated in KIT+ BMMC (blue signature), the 76 genes selectively up-regulated in KIT- BMMC (green signature), and the 34 genes up-regulated in both BMMC (turquoise signature) featuring *Il1b* (red font). C Normalized microarray expression values of top genes with human orthologues from each signature compared with *Gusb* control ($n = 2$ /data point). D qPCR data summary of *Il1b* normalized to *Gusb* expression of KIT+ and KIT- BMMC upon 24-h incubation with cell-free LLC-CM ($n = 3$). Data are shown as Tukey's whiskers (boxes: interquartile range; bars: 50% extreme quartiles). ***: $P < 0.001$ for LLC-CM-treated KIT+ BMMC compared with all other groups by two-way ANOVA with Bonferroni post-tests. Only statistically significant differences are indicated. E KIT+ and KIT- BMMC were assessed for caspase-1 (CASP1) and β -actin (ACTB) immunoreactivity by Western immunoblot upon 24-h incubation with DMEM (-) or cell-free LLC-CM (+). F Representative cytocentrifugal specimens of IL-1 β immunostained and toluidine blue counter-stained KIT+ and KIT- BMMC upon 24-h incubation with DMEM or cell-free LLC-CM. G Data summary from (F). Data are shown as Tukey's whiskers (boxes: interquartile range; bars: 50% extreme quartiles). ***: $P < 0.001$ for LLC-CM-treated KIT+ BMMC compared with all other groups by two-way ANOVA with Bonferroni post-tests. Only statistically significant differences are indicated. H *C57BL/6* and *Il1b*^{-/-} mice on the *C57BL/6* background ($n = 5$ /group), received 10^6 subcutaneous Lewis lung carcinoma cells (LLC) and were followed for one month by weekly measurement of three vertical primary tumor diameters (δ) and calculation of primary flank tumor volume ($V = \pi\delta^3/6$). Data summary of primary subcutaneous tumor volume expressed as percentage of *C57BL/6* controls (mean \pm SEM) with two-way ANOVA P value.

KIT+ MC. Hence, this report presents the first direct evidence for a requirement for KIT+, IL-1 β -competent mast cells in *KRAS*-mutant LADC, identifying new targets for therapy.

The results favor an important role for MC during the whole spectrum of LADC formation, progression, and metastasis.³⁵ To this end, MC-deficient mice were protected from direct tumor initiation of the airway and alveolar epithelium using

the tobacco carcinogen urethane and oncogenic *KRAS*^{G12D} respectively, and were also resistant to the heterotopic growth of established LADC in the skin, as well as to its spontaneous metastasis back to the lungs. MC are known to heavily colonize the airways of mice and men,^{12–19,29} where tumor initiation by environmental carcinogens occurs,^{1,37} and were shown here to progressively infiltrate LADC of increasing stage, positioning

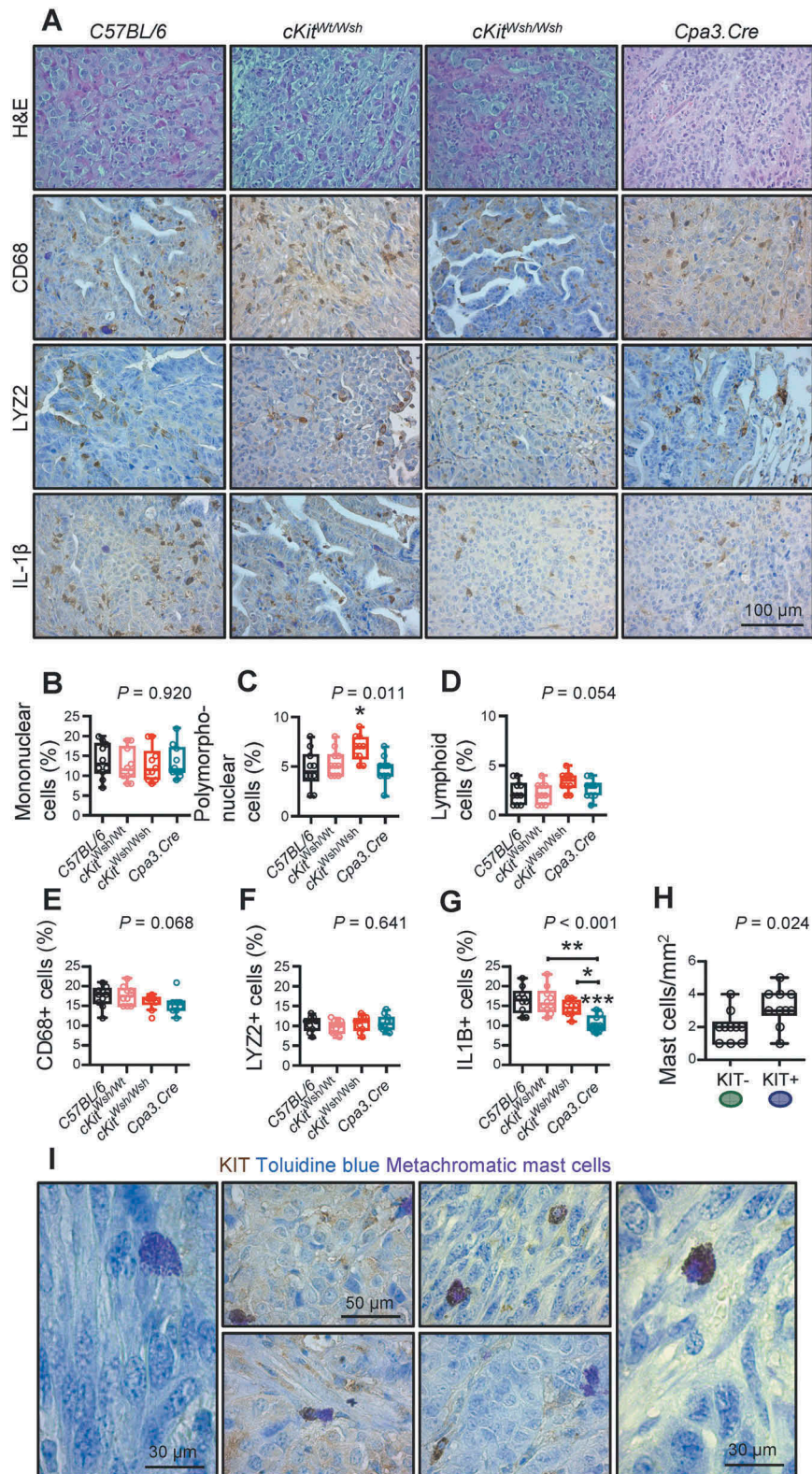


Figure 7. Lung adenocarcinoma microenvironment of mast cell-competent and incompetent mice.

A Representative images of lung adenocarcinomas from Figures 3–5 ($n = 10$ mice/group randomly chosen from the urethane, *KRAS*^{G12D} and heterotopic models) stained with hematoxylin and eosin (H & E) or immunostained with anti-CD68, anti-LYZ2, and anti-IL-1 β antibodies and counterstained with toluidine blue. B–G Data summary from (A). Data are shown as Tukey's whiskers (boxes: interquartile range; bars: 50% extreme quartiles), raw data points (dots), and Kruskal–Wallis ANOVA P values. Comparisons shown are: * $P < 0.05$ for comparisons with C57BL/6 controls or as indicated by Dunn's post-tests. Only statistically significant differences are indicated. H Representative lung adenocarcinomas from Figures 3–5 ($n = 10$ mice/group randomly chosen from the urethane, *KRAS*^{G12D} and heterotopic models) were immunostained with anti-KIT antibody and counterstained with toluidine blue. Data summary shown as Tukey's whiskers (boxes: interquartile range; bars: 50% extreme quartiles), raw data points (dots), and Mann–Whitney u -test P value. I Representative images of LADC-infiltrating KIT+ (left) and KIT- (right) MC and their colocalization in tumors (middle).

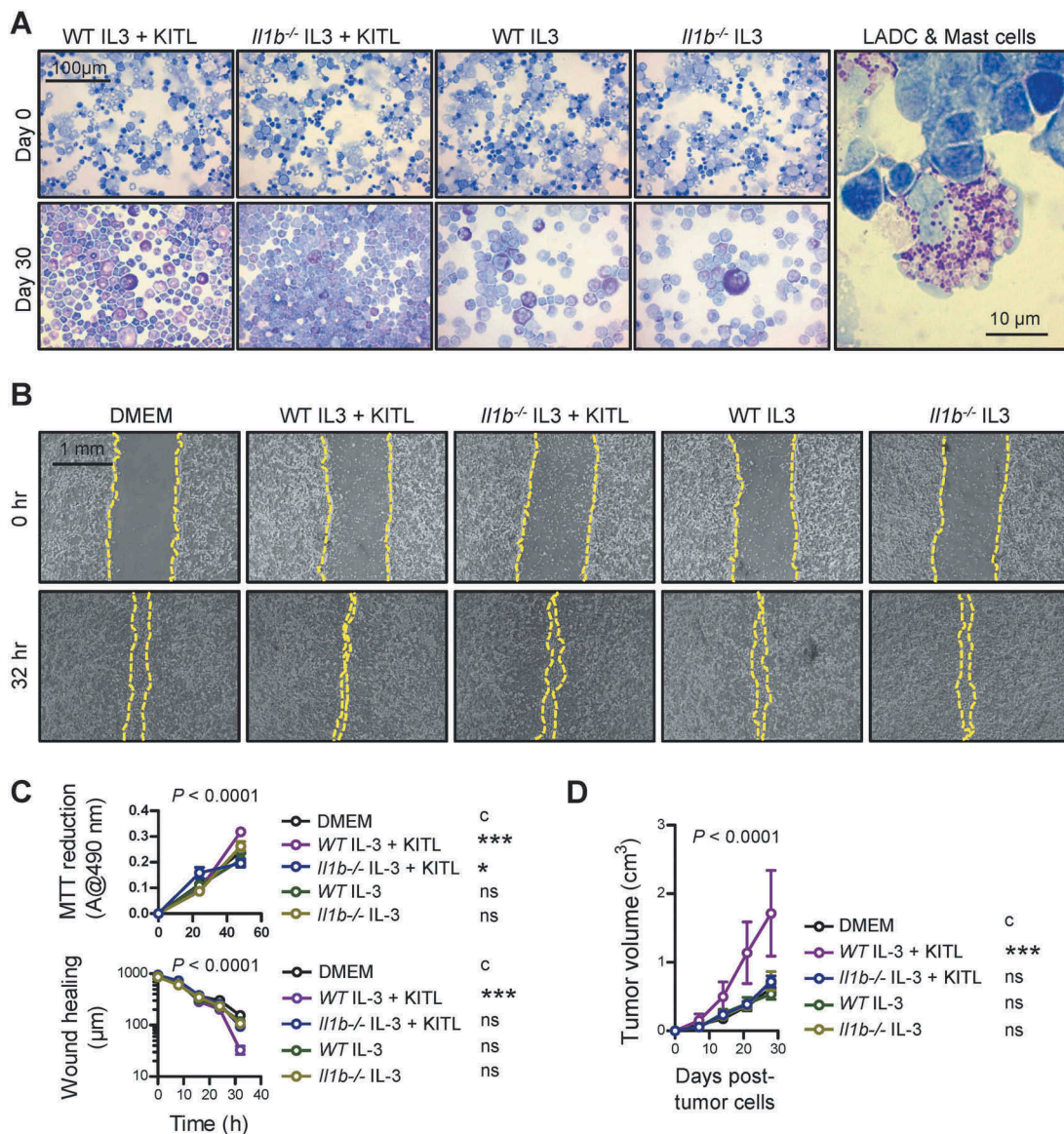


Figure 8. KIT-dependent mast cells competent in interleukin-1 β are required for lung adenocarcinoma.

A *Left*: Representative cytocentrifugal specimens of toluidine blue-stained bone marrow-derived cells from WT and *Il1b*^{-/-} mice before (top) and after one-month incubation with 100 μ g/mL interleukin (IL)-3 and 100 μ g/mL KIT ligand (KITL) or with 100 μ g/mL IL-3 alone (bottom). Note the >95% metachromasia of bone marrow-derived mast cells (BMMC) of different maturation stages after treatment. *Right*: Representative cytocentrifugal specimen of toluidine blue-stained BMMC mixed with LLC cells at 1:50 ratio before experiments. B, C LLC cells alone or co-cultured with BMMC from (A) were assessed for *in vitro* cellular proliferation by MTT reduction and for *in vitro* cell migration by scratch assay. (B) Representative scratch assay images at experiment start and conclusion. (C) Summary of data from $n = 5$ –6 independent experiments expressed as mean \pm SEM with two-way ANOVA P values. ns, *, and ***: $P > 0.05$, $P < 0.05$, and $P < 0.001$, respectively, for comparison with DMEM control (c) by Bonferroni post-tests. D *Ccr2* gene-deficient mice ($n = 6$ /group) received 10^6 subcutaneous LLC cells alone or mixed with BMMC at 50:1 ratio and were followed for a month by weekly measurements of three vertical primary tumor diameters and calculation of flank tumor volume. Summary of data from $n = 6$ mice/group expressed as mean \pm SEM with two-way ANOVA P value. ns and ***: $P > 0.05$ and $P < 0.001$, respectively, for comparison with DMEM control (c) by Bonferroni post-tests.

MC as plausible effectors of LADC development and progression. The results also favor a ubiquitous LADC-promoting role for MC across anatomical compartments of the lungs, since MC-deficient mice were protected from both airway- and alveolar-inflicted LADC.^{36,38} This is important given the diversity of the cellular origin of LADC in mice and humans if MC-based therapy is ever contemplated.^{35–39}

But how can the divergent results from urethane-treated *cKit*^{W^{sh}} and *Cpa3.Cre* mice be explained? We believe that the results do not contradict the proposed tumor-promoting role for MC in LADC and can be explained on several counts. First,

cKit^{W^{sh}} mice were not completely devoid of airway MC, and we recently showed urethane-induced tumors to stem from the airways.³⁶ Second, urethane-caused LADC were less infiltrated by MC compared with *KRAS*^{G12D} and LLC tumors, likely reflecting their more early nature compared with the other models,^{37,40,43} and probably dictating their lesser dependence from MC. This assumption is in line with the increasing MC infiltrates of advanced human LADC, as well as the more profound impact of MC deficiency in mouse models of more advanced disease like the *KRAS*^{G12D} and LLC model shown here and the malignant pleural effusion models shown elsewhere.³³

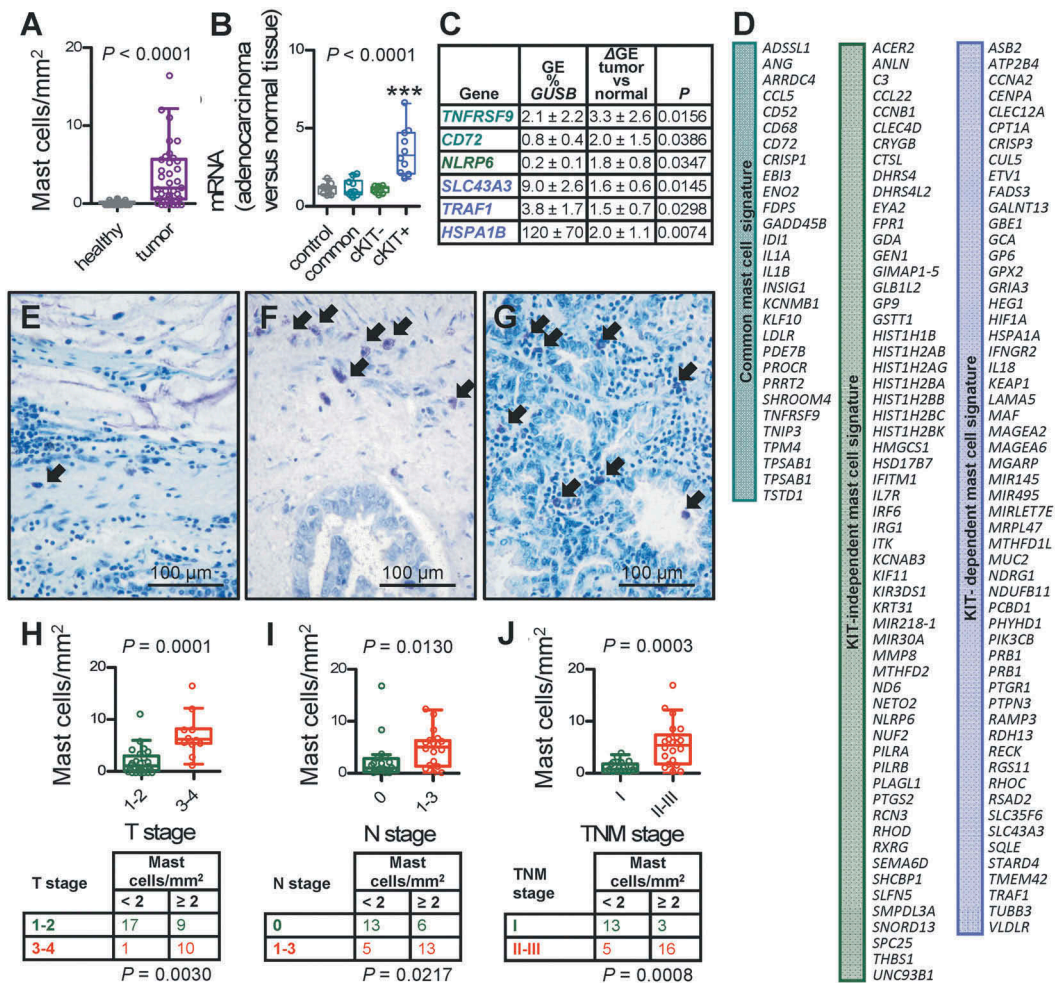


Figure 9. Mast cells and mast cell signatures in human lung adenocarcinoma.

A Data summary of mast cell (MC) density of 37 patients with lung adenocarcinoma.⁵⁰ Data are shown as Tukey's whiskers (boxes: interquartile range; bars: 50% extreme quartiles), raw data points (dots), and paired Student's t-test P value. Full patient data are provided in Table 1. B Data summary of gene expression (GE) levels of the human orthologues of the murine MC signatures identified in Figure 6 relative to *GUSB* and *HPRT* (control) of tumor and adjacent normal-appearing lung tissues of 10 patients with lung adenocarcinoma.⁵² Blue: KIT-dependent MC signature; green: KIT-independent MC signature; turquoise: common MC signature. Data are shown as Tukey's whiskers (boxes: interquartile range; bars: 50% extreme quartiles), raw data points (dots), and repeated measures ANOVA P value. ***: $P < 0.001$ for comparison with all other groups by repeated measures ANOVA with Bonferroni post-tests. Full patient data are provided in Table 2. C Select transcripts from the three signatures from (B) significantly over-represented in tumor versus adjacent normal-appearing lung tissues with GE versus *GUSB*, differential GE (Δ GE) of tumor tissue versus normal lung, and P values by paired Student's t-test. D The human orthologues of the three murine MC signatures identified in Figure 6. E-G Representative toluidine blue-stained tissue sections showing purple mast cells (arrows) in primary lung adenocarcinomas of a 68-year-old female with stage T₂N₀M₀ disease featuring 3.6 mast cells/mm², a 51-year-old male with T₂N₁M₀ disease displaying 11.2 mast cells/mm², and a 64-year-old male with T₄N₀M₀ disease exhibiting 16.6 mast cells/mm². H-J Data summary (graphs) and frequency distribution (tables) of mast cell density of 37 patients with lung adenocarcinoma,⁵⁰ classified by T, N, and TNM stage according to the sixth edition of the TNM staging system.⁶³ Data are shown as Tukey's whiskers (boxes: interquartile range; bars: 50% extreme quartiles), raw data points (dots), n (tables), and Mann-Whitney u-test (graphs) and Fischer's exact (tables) P values. Full patient data are provided in Table 1.

Third, rebound immune responses are at play in *cKit*^{Wsh} mice, such as myeloid suppressor and regulatory T cell expansion,^{47,57} cell types we have previously shown to promote early urethane-induced and advanced LADC.^{43,58} Finally, as the founders of *Cpa3.Cre* mice and our group previously showed,^{27,33} these mice represent truly and exclusively MC-deficient models that behave differently compared with *cKit*^{Wsh} mice in response to various challenges,²⁷ rendering the results from this strain more closely related to MC function and not to KIT signaling. To this end, *Cpa3.Cre* mice were ubiquitously protected from urethane, as well as from LLC tumors and their metastases, corroborating the requirement for MC in LADC.

The data presented here are novel and unprecedented and explain previous clinical and preclinical observations and

in vitro functional findings.²⁸⁻³¹ Our *in vivo* results are important additions to the field, since MC play divergent tumor-promoting or gate-keeping roles in different cancers.^{20-23,33} The reasons for this may be multiple, including the different tumor models employed and the multifaceted phenotypes of MC in the various bodily anatomic compartments.^{15,17,27,33,44} Whatever the impact of these cells in other tumor types, the results shown here establish for the first time KIT+ MC as culprits of *KRAS*-mutant LADC promotion and as candidate therapeutic targets against a disease that presents a current pandemic.^{1,2} In addition to identifying their role and to providing mechanistic insights, we describe gene sets that may mediate LADC promotion by MC for future research. These signatures include *IL1B*, *TNFRSF9*, *CD72*, *NLRP6*, *SLC43A3*, *TRAF1*,

Table 1. Clinical data and mast cell density of 37 patients with lung adenocarcinoma from Patras, Greece.⁵⁰ No patient had metastasis (M₀ for all).

#	Gender	Age (years)	Histologic subtype(s)	Grade (1–3)	TNM			Mast cells/mm ²
					T	N	TNM	
1	M	60	Solid	1	4	1	IIIb	5,4
2	M	73	Acinar	2	2	0	Ib	2,8
3	M	56	Solid/papillary	3	3	1	IIIa	5,6
4	M	68	Micropapillary	3	1	0	Ia	2
5	M	63	Acinar	2	2	0	Ib	0,4
6	M	63	Acinar/papillary	2	2	0	Ib	0
7	M	63	Solid	3	2	1	IIb	2,2
8	M	67	Acinar (cribriform)	3	1	0	Ia	0
9	M	62	Acinar	2	2	1	IIb	4,6
10	M	72	Acinar/solid	3	2	1	IIb	0
11	M	66	Acinar/solid	3	4	1	IIIb	1,4
12	F	55	Acinar	1	2	1	IIb	4,4
13	M	64	Acinar	3	2	1	IIb	4
14	M	53	Acinar	1	1	0	Ia	0,2
15	M	64	Lepidic/acinar/micropapillary	3	4	0	IIIb	16,6
16	M	70	Acinar	2	1	1	Ia	1,2
17	M	50	Solid	3	2	1	IIb	0
18	M	51	Acinar/micropapillary	3	2	1	IIb	11,2
19	M	68	Solid	3	3	1	IIIa	5,8
20	M	69	Micropapillary/acinar	2	3	1	IIIa	6,6
21	M	53	Acinar	2	1	0	Ia	0,4
22	M	49	Acinar	2	1	0	Ia	1,8
23	M	72	Solid	2	1	0	Ia	0,8
24	M	60	Solid	2	2	0	Ib	0
25	M	58	Acinar	3	2	0	Ib	1,8
26	M	71	Acinar	3	2	0	Ib	1
27	F	53	Solid	2	3	0	IIb	3
28	M	59	Colloid	1	3	1	IIIa	8,2
29	M	72	Acinar	2	2	1	IIb	6
30	M	54	Acinar	3	3	0	IIb	8,2
31	M	62	Solid	2	1	0	Ia	0
32	F	67	Solid	3	2	1	IIb	0,8
33	M	58	Solid	3	3	1	IIIa	6,2
34	M	54	Acinar/solid	2	1	0	Ia	0,8
35	M	69	Solid	3	3	1	IIIa	12,2
36	F	68	Colloid	2	2	0	Ib	3,6
37	M	65	Papillary/acinar	2	1	0	Ia	1,4

HSPA1B, and other genes of the KIT+ MC signature, genes likely important for MC expansion in tumor tissues, MC signal transduction upon tumor cell encounter, inflammasome activation, transmembrane transport, and telomere maintenance, and may promote further research on tumor-associated MC functions in the future. To this end, MC-derived IL-1 β can fuel transcriptional activity of nuclear factor- κ B in tumor cells.^{33,34} Our results may explain the findings of the Canakinumab Anti-inflammatory Thrombosis Outcomes Study (CANTOS) aiming at prevention of cardiovascular events using the IL-1 β -neutralizing antibody canakinumab.^{59,60} After three years of

intervention, CANTOS investigators detected biologically and statistically significant reductions in overall and lung cancer incidence, findings consistent with the protumorigenic role of IL-1 β reported here and elsewhere.^{33,34}

In conclusion, KIT-dependent mast cells were found here to fuel *KRAS*-mutant lung adenocarcinoma formation, growth, and metastasis in mice by secreting IL-1 β and to be associated with lung adenocarcinoma progression in humans, setting a rational framework for further study of mast cell functions in lung tumors.

Materials and methods

Cells

Lewis lung carcinoma (LLC; NCI Tumor Repository, Frederick, MD) cells were cultured at 37°C in 5% CO₂-95% air using DMEM supplemented with 10% FBS, 2 mM L-glutamine, 1 mM pyruvate, 100 U/ml penicillin, and 100 mg/ml streptomycin. Cells were tested biannually for identity (by the short tandem repeat method) and for *Mycoplasmaspp.* (by PCR). For *in vivo* injections, cells were harvested using trypsin, incubated with Trypan blue, and counted.³³ Only 95% viable cells were used *in vivo*. BMMC were derived from bone marrow cells flushed from mouse femurs and tibias using full DMEM after one month of culture in full culture media, supplemented with 100 ng/mL IL-3 alone or 100 ng/mL IL-3 plus 100 ng/mL KITL.³³ LLC cells alone or co-cultured with BMMC at a ratio of 50:1 were assessed for cellular proliferation by MTT reduction and cell migration *in vitro* with scratch assay for 48 and 32 h respectively. This LLC:BMMC ratio was selected as physiologically relevant based on *in vivo* MC densities observed in all three tumor models employed herein.

Mouse models

C57BL/6 (#000664), *B6.129P2-Lyz2^{tm(Cre)Ifo}/J*(#004781),⁴⁵ *B6.129S4-Ccr2^{tm11fc}/J*(#004999),⁴⁷ *B6.129S4-Kras^{tm4Tyj}/J* (*KRAS*^{G12D} #008179),⁴⁰ and *B6.Cg-Kit^{W-sh}/HNIhrJaeBs mGllj* (*cKit^{W-sh}*; #012861)⁴⁴ mice were from Jackson Laboratory (Bar Harbor, MN), *Cpa3.Cre* mice were a gift from Dr. HR Rodewald, University of Heidelberg, Germany,²⁷ and *Il1b*-deficient mice from Dr. Y Iwakura, Tokyo University of Science, Tokyo, Japan.⁴⁸ All mice were bred at the Center for Animal Models of Disease of the Department of Physiology at the Faculty of

Table 2. Clinical data and mast cell signature gene expression data of 10 patients with lung adenocarcinoma from Borstel, Germany.⁵²

#	Gender	Age (years)	Grade (1–3)	T	N	M	TNM	Normalized expression of mast cell signature genes in lung adenocarcinoma compared with adjacent normal-appearing lung tissue (fold control genes <i>GUSB/HPRT</i>)			
								control	common	cKIT-	cKIT+
1	F	61	3	3	1	0	IIIa	1,44	0,89	0,99	2,12
2	M	69	3	3	3	0	IIIb	1,11	0,79	1,22	1,77
3	F	66	3	3	0	0	IIb	0,82	0,55	1,28	6,59
4	F	58	3	2	2	1	IV	1,77	0,90	0,92	2,02
5	F	71	3	4	2	0	IIIb	1,23	0,92	1,10	3,05
6	M	74	3	3	2	0	IIIa	0,72	0,71	1,21	4,67
7	F	54	3	4	3	0	IIIb	1,19	1,53	0,72	4,81
8	F	53	3	3	0	0	IIb	0,69	2,06	0,80	3,48
9	F	74	2	2	2	0	IIIa	1,20	1,43	1,31	2,68
10	F	57	2–3	1	0	0	Ia	1,13	1,97	1,25	4,12

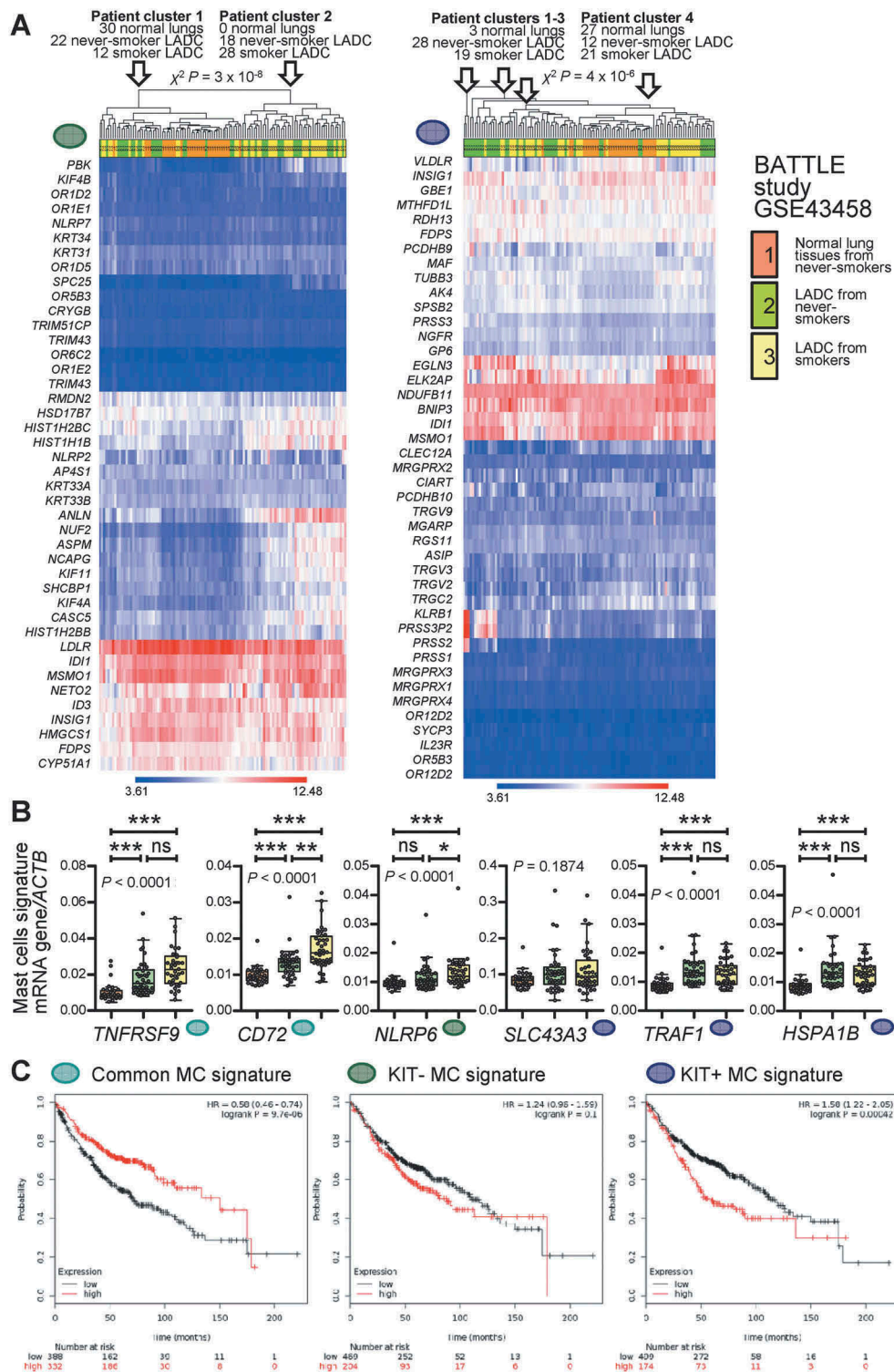


Figure 10. Mast cell signatures in human lung adenocarcinoma.

A Unsupervised clustering of 30 normal lung tissues from never-smokers (orange), 40 lung adenocarcinoma (LADC) tissues from never-smokers (green), and 40 LADC tissues from smokers (yellow) from the Biomarker-integrated Approaches of Targeted Therapy for Lung Cancer Elimination (BATTLE) study [Gene Expression Omnibus (GEO) dataset GSE43458; freely available at <https://www.ncbi.nlm.nih.gov/geo/query/acc.cgi?acc=GSE43458>]⁵¹ by the humanized KIT-independent (left) and KIT-dependent (right) mast cell (MC) signatures from Figure 9D. Both signatures could accurately discriminate normal lung from LADC tissues. P , exact χ^2 probability values calculated at <http://courses.atlas.illinois.edu/spring2016/STAT/STAT200/pchisq.html>. B Data summary of gene expression of the transcripts from Figure 9C normalized to *ACTB* expression in the BATTLE study validates five of the six genes. Color code is as in Figure 10A. Data are shown as Tukey's whiskers (boxes: interquartile range; bars: 50% extreme quartiles), raw data points (dots), and Kruskal-Wallis ANOVA P values. ns, *, **, and ***: $P > 0.05$, $P < 0.05$, $P < 0.01$, and $P < 0.001$, respectively, for the indicated comparisons by Dunn's post-tests. C Overall survival of patients with LADC stratified by low (black lines) or high (red lines) average expression of the MC signatures from Figure 9D. Data from <http://kmplot.com/analysis/index.php?p=service&cancer=lung>.⁵⁴ Note that exclusively high expression of the KIT-dependent MC signature correlates with poor survival (A). Shown are Kaplan-Meier survival estimates with hazard ratios (HR) for high compared with low signature expression with their 95% confidence intervals, as well as log-rank test P values.

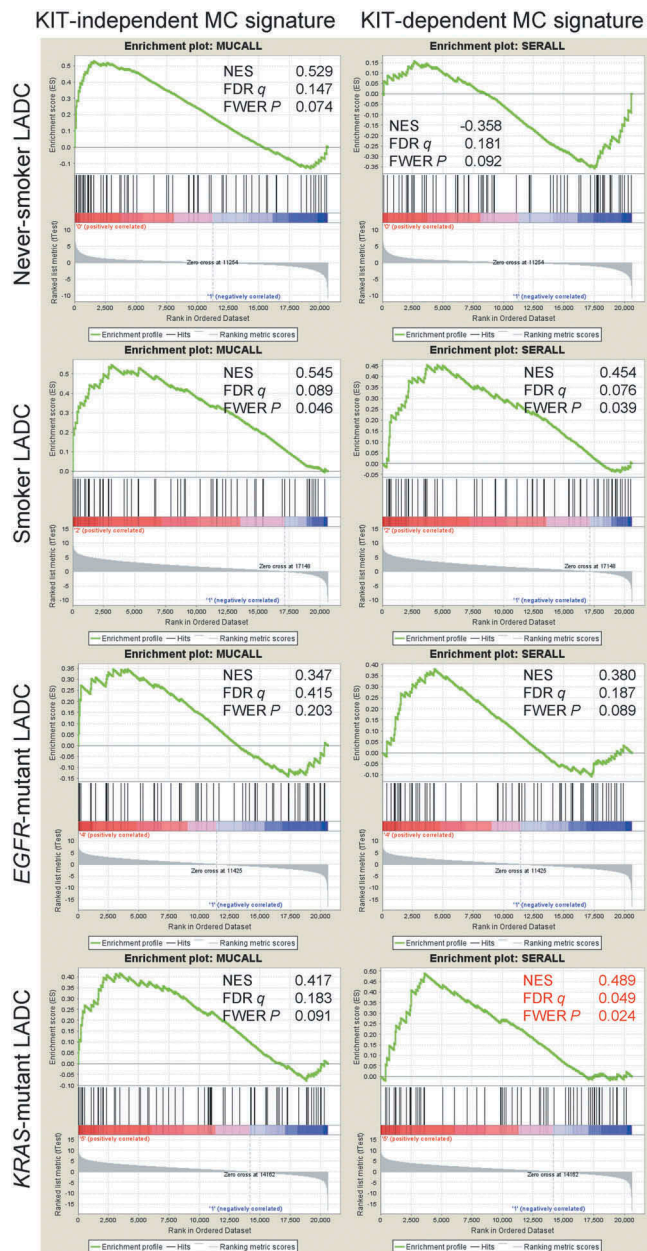


Figure 11. The KIT-dependent mast cell signature is focally enriched in KRAS-mutant lung adenocarcinoma.

Pre-ranked gene set enrichment analysis of the humanized KIT-independent (left) and KIT-dependent (right) mast cell (MC) signatures from Figure 9D against 40 lung adenocarcinoma (LADC) tissues from never-smokers, 40 LADC tissues from smokers, 15 *EGFR*-mutant LADC, and 22 *KRAS*-mutant LADC from the Biomarker-integrated Approaches of Targeted Therapy for Lung Cancer Elimination (BATTLE) study [Gene Expression Omnibus (GEO) datasets GSE43458 and GSE31852; freely available at <https://www.ncbi.nlm.nih.gov/geo/query/acc.cgi?acc=GSE43458> and <https://www.ncbi.nlm.nih.gov/geo/query/acc.cgi?acc=GSE31852>].^{53,55,56} GSEA was performed with the Broad Institute pre-ranked GSEA module software (<http://software.broadinstitute.org/gsea/index.jsp>).⁶⁵ Normal lung tissue from 40 never smokers were used as controls (GSE31852). Note that using stringent cut-offs of both false discovery rate (FDR) q values <0.05 and family-wise error rate (FWER) probability (P) values <0.05 the KIT-dependent MC signature is focally enriched in the molecular signature of *KRAS*-mutant LADC (red fonts). Shown are enrichment plots, normalized enrichment scores (NES), FDR, and FWER values.

Medicine of University of Patras, Greece. Experiments were approved by the Veterinary Administration of the Prefecture of Western Greece (#118018/578/30.04.2014)

and were conducted according to Directive 2010/63/EU (<http://eurlex.europa.eu/legal-content/EN/TXT/?uri=CELEX%3A32010L0063>). Male and female mice were sex-, weight (20–25 g)-, and age (6–12 week)-matched. For LADC induction using the pulmonary carcinogen urethane (ethyl carbamate, EC; CAS #51–79–6; Sigma, St. Louis, MO), mice on the *C57BL/6* background received 10 weekly intraperitoneal injections (1g/Kg per 100 μ l saline prepared on the same day) and were sacrificed 6 months after the first injection.³⁷ For mutant *KRAS*^{G12D}-driven LADC, *C57BL/6* mice heterozygous for the loxP-STOP-loxP.*KRAS*^{G12D} transgene (*KRAS*^{G12D} mice), which express mutant *KRAS*^{G12D} in all somatic cells upon CRE-mediated recombination, received 5 \times 10⁸ intratracheal plaque-forming units (pfu) adenovirus encoding CRE recombinase (*Ad-Cre*; Baylor College of Medicine, Houston, TX) and were killed after four months.⁴⁰ Control mice (designated *C57BL/6*) were a mixture of littermates negative for the transgenes of interest, including *cKit*^{Wt/Wt} mice as appropriate controls for *cKit*^{Wsh} mice and *Lyz2.Cre* mice as appropriate controls for *Cpa3.Cre* mice.⁴⁵ *C57BL/6* mice were anesthetized by isoflurane and received 10⁶ LLC cells alone or combined with 2 \times 10⁴ BMMC subcutaneously into the rear flank. The 50:1 ratio of co-injected LLC and BMMC cells was chosen in order to replicate the number of MC in LADC MC hotspots. Three vertical tumor diameters (δ) were measured weekly, tumor volume (V) was calculated as $V = \pi \times (\delta_1 \times \delta_2 \times \delta_3) / 6$, and mice were killed after one month.⁴³ Lungs were exsanguinated, inflated at 20 cm H₂O with 10% neutral-buffered formalin, and fixed overnight. Lung tumor number and δ were measured under a Stemi DV4 stereoscope (Zeiss; Jena, Germany) and V was calculated as $\pi \delta^3 / 6$ and averaged/summed. Lung volume was measured by saline immersion, lungs were embedded in paraffin, randomly sampled by 5 μ m-thick sections ($n = 10$ /lung), mounted on glass slides, and stained with hematoxylin and eosin (H&E). A 100-point-grid was superimposed on ≥ 5 random non-overlapping fields of ≥ 10 sections/lung using Fiji (<https://fiji.sc/>) and lung tumor burden was determined by extrapolating tumor-to-lung point counts to lung volume.^{61,62}

Quantification of lung tumors

Specimens were examined by two blinded participants of this study and the results obtained by each investigator were compared and re-evaluated if deviant by >20%. In the urethane and lung metastasis models, tumors are approximately spherical with well-defined borders. Lungs and lung tumors were thus inspected macroscopically under a Stemi DV4 stereoscope equipped with a micrometric scale incorporated into one eyepiece and an Axiocam ERC5s camera (Zeiss, Jena, Germany) in transillumination mode, allowing for visualization of both superficial and deeply located lung tumors.³⁷ Tumor location was charted and δ was measured. Tumor number (multiplicity) per mouse was counted and mean tumor δ per mouse was calculated as the average of individual δ of all tumors found in a given mouse lung.

Individual tumor volume was calculated as $\pi\delta^3/6$. Mean tumor volume per mouse was calculated as the average of individual volumes of all tumors found in a given mouse lung, and total lung tumor burden per mouse as their sum. In the *KRAS*^{G12D} model, lung tumors are irregularly shaped with ill-defined borders. Hence, lung volume was measured by saline immersion, and lungs were embedded in paraffin, randomly sampled by cutting 5 μm -thick lung sections, mounted on glass slides, and stained with hematoxylin and eosin for morphometry. For this, a digital grid of 100 intersections of vertical lines (points) was superimposed on multiple digital images of all lung sections from lung tissue of a given mouse using Fiji.⁶¹ Total lung tumor burden was determined by point counting of the ratio of the area occupied by neoplastic lesions versus total lung area and by extrapolating the average ratio per mouse to total lung volume.⁶² The results of this stereologic approach were compared with the macroscopic method detailed above and were scrutinized if deviant by >20%. All quantifications were done by counting at least five random non-overlapping fields of view of at least 10 sections per lung.

Human samples

Matched tumor and normal lung tissue of 37 previously reported patients with LADC treated at the Faculty of Medicine of the University of Patras, Greece were used for MC counts,⁵⁰ and of 10 previously reported patients with LADC treated at the Research Center Borstel of the Airway Research Center North, Germany for microarray.⁵² Patients were staged according to the sixth edition of the tumor-node-metastasis system for lung cancer.⁶³

Histology

Five μm -thick tissue sections were stained with H&E or with toluidine blue (pH = 2.0; 10 min; RT; Sigma, St. Louis, MO) or were incubated with primary antibodies (Table 3) overnight at 4 °C followed by Envision/diaminobenzidine detection (Dako, Glostrup, Denmark) and hematoxylin or toluidine blue counterstaining/mounting (Entellan; Merck, Darmstadt, Germany). Nuclear PCNA immunoreactivity was defined as the percentage of positive cells in tumor areas. Sections were counted at high power (x 400) and 5–8 fields were assessed randomly for tumor cells. One thousand cell nuclei were counted and the number of cells showing positive nuclear staining was recorded. KIT, CD68, and LYZ2 immunoreactivity were defined as the

percentage of positive cells. IL-1 β immunostaining intensity was defined semiquantitatively (0: negative; 1: weak; 2: moderate; 3: strong). To assess the number of MC, slides were scanned at low power (x 20) to identify the 10 fields with the greatest number of MC (hotspots) separately in control lung tissue and in LADC. MC number was counted at high power (x 200) in every hotspot and the average was determined. Perivascular areas, where mast cells naturally accumulate, were excluded. Mononuclear, polymorphonuclear, and lymphocytic infiltrates were identified morphologically from H&E staining in 10 fields at a magnification of x 400 and the average was determined. Images were captured with an AxioLab.A1 upright microscope (Zeiss, Jena, Germany). Staining was evaluated by two blinded readers (IG, IL) and was verified by a certified pathologist (VB).

qPCR

RNA was isolated using Trizol (Invitrogen, Carlsbad, CA) followed by RNAeasy (Qiagen, Hilden, Germany), was reverse transcribed using Superscript III (Invitrogen), and qPCR was performed using SYBR Green Master Mix and specific primers for *I11b* (I11bF: TTTGACAGTGATGAGAATGACC; I11bR: AATGAGTGATACTGCCTGCC; *GusbF*: TTACTTTAAGACGCTGATCACC; *GusbR*: ACCTCCAAATGCCCATAGTC) in a StepOne Plus thermocycler (Applied Biosystems, Carlsbad, CA). Ct values from triplicate qPCR reactions were analyzed by the $2^{-\Delta\Delta\text{CT}}$ method relative to *Gusb* mRNA levels.⁶⁴

Immunoblotting

Total protein extracts from BMBC were extracted using Radioimmunoprecipitation assay buffer (Thermo Fisher Scientific, Waltham, MA), were separated by 12% SDS polyacrylamide gel electrophoresis, and were electroblotted to polyvinylidene difluoride membranes (Merck Millipore, Darmstadt, Germany). Membranes were probed with anti-CASP1 and anti- β -Actin (ACTB) antibodies (Table 3) and were visualized by film exposure after incubation with enhanced chemiluminescence substrate (Merck Millipore, Darmstadt, Germany).

Transcriptome analyses

Microarray data were analyzed with Gene Expression and Transcriptome Analysis Consoles using as cut-off differential gene expression > 2 (Affymetrix, Santa Clara, CA). Murine BMBC microarrays were reported elsewhere (GEO series GSE58189; <https://www.ncbi.nlm.nih.gov/geo/query/acc.cgi?acc=GSE58189>).³³ Humanized MC signatures were derived from mouse BMBC signatures using Orthoretriever (<http://lighthouse.ucsf.edu/orthoretriever/>).⁵¹ Hierarchical clustering of BATTLE study patients by MC signatures was performed using GEO series GSE43458.⁵³ Human LADC patient survival analyses were done using Kaplan–Meier Plotter (<http://kmplot.com/analysis/index.php?p=service&cancer=lung>) and parameters auto-select best cutoff, compute median survival, censor at threshold, and histologic subtype lung adenocarcinoma.⁵⁴ GSEA was performed with the Broad Institute pre-ranked GSEA module (<http://software.broadinstitute.org/gsea/index>).

Table 3. Antibodies used for immunohistochemistry.

Product name/Target	Host species	Provider	Catalog#	Dilution
Anti-proliferating cell nuclear antigen antibody (PCNA)	Rabbit	Abcam, London, UK	ab2426	1:2000
Anti-CD68 antibody (CD68)	Mouse	Abcam, London, UK	ab955	1:200
Anti-Lysozyme antibody (LYZ2)	Rabbit	Abcam, London, UK	ab10850	1:250
Anti-Interleukin-1 β antibody (IL-1 β)	Rabbit	Abcam, London, UK	ab9722	1:200
Anti c-KIT (c-Kit)	Mouse	Santa Cruz Biotechnology, INC	sc-365504	1:100

jsp) using BATTLE study transcriptomes from GEO series GSE43458 and GSE31852.⁶⁵

Statistics

Sample size (n ; always biological) was determined using G^* power,⁶⁶ assuming $\alpha = 0.05$, $\beta = 0.05$, and Cohen's $d = 1.5$. Data were acquired by two blinded readers, reevaluated if >20% deviant (no data were excluded), examined for normality by Kolmogorov–Smirnov test, and presented as median (interquartile range) or mean \pm SEM. Differences in frequencies were examined by Fischer's exact or χ^2 tests, in means of normally distributed variables by t-test or one-way ANOVA/Bonferroni post-tests, and in medians of non-normally distributed variables by Mann–Whitney test or Kruskal–Wallis/Dunn's posttests. Survival and flank tumor volume were examined by Kaplan–Meier estimates/log-rank tests and two-way ANOVA/Bonferroni post-tests. Probability (P) is two-tailed and $P < 0.05$ was considered significant. Statistics and plots were done on Prism v5.0 (GraphPad, La Jolla, CA).

Study approval

All animal experiments were approved *a priori* by the Veterinary Administration of the Prefecture of Western Greece according to a full and detailed protocol (approval number 118018/578/30.04.2014) and were conducted according to Directive 2010/63/EU (<http://eurlex.europa.eu/legal-content/EN/TXT/?uri=CELEX%3A32010L0063>). Human studies were approved *a priori* by the Ethics Committee of the University of Lübeck, Germany (approval # AZ 12–220),⁵² and by the ethics committee of the University Hospital of Patras, Greece.⁵⁰ The study's protocols were conducted according to the Declaration of Helsinki and all patients gave written informed consent.

Acknowledgments

The authors thank the University of Patras Center for Animal Models of Disease for experimental support, Dr. Hans-Reimer Rodewald for kindly providing *Cpa3.Cre* mice, and Dr. Yoichiro Iwakura for kindly providing *Il1b*-deficient mice. This work was supported by European Research Council 2010 Starting Independent Investigator and 2015 Proof of Concept Grants (260524 and 679345, respectively, to GTS), a Hellenic State Scholarships Foundation (Ίδρυμα Κρατικών Υποτροφιών, IKY) Research Fellowship 2015–16 (to IL) and by Greek National Funds through the action National Science and Research Foundation (NSRF) 2014–2020 “Reinforcement of Postdoctoral Researchers” (to IG).

Authors' contributions

IL performed most *in vivo* experiments, histology and microscopy, analyzed the data, designed the study and wrote the draft of the manuscript; GN performed pilot *in vivo* experiments, histology and microscopy; VP performed pilot *in vivo* experiments; GAG performed GSEA; MO, AM, and MS performed *in vivo* experiments, genotyping, cell culture, RNA isolation, tumor cell and carcinogen injections, and tissue processing; SM and TG performed and analyzed human microarrays; VB analyzed human lung adenocarcinomas for mast cell content and provided expert pathologic advice; GTS and IG designed and guided the study, analyzed the data and wrote the final version of the manuscript. GTS also funded the study, is the guarantor of the study's integrity, and wrote/designed the final paper/

figure set submitted. All authors critically reviewed and edited the paper for important intellectual content and approved the final submitted version.

Disclosure of Potential Conflicts of Interest

No potential conflicts of interest were disclosed.

Funding

This work was supported by the European Research Council [260524, 679345], Hellenic State Scholarships Foundation.

ORCID

Vassilios Papaleonidopoulos  <http://orcid.org/0000-0001-7324-9796>
Ioanna Giopanou  <http://orcid.org/0000-0003-4393-7517>
Georgios T. Stathopoulos  <http://orcid.org/0000-0002-9215-6461>

References

- Alberg AJ, Ford JG, Samet JM, American College of Chest Physicians. Epidemiology of lung cancer: ACCP evidence-based clinical practice guidelines (2nd edition). *Chest*. 2007;132(3 Suppl):29S–55S. doi:10.1378/chest.07-1347.
- Torre LA, Bray F, Siegel RL, Ferlay J, Lortet-Tieulent J, Jemal A. Global cancer statistics, 2012. *CA Cancer J Clin*. 2015;65(2):87–108. doi:10.3322/caac.21262.
- Cancer Genome Atlas Research Network. Comprehensive molecular profiling of lung adenocarcinoma. *Nature*. 2014;511(7511):543–550. doi:10.1038/nature13385.
- Houghton AM. Mechanistic links between COPD and lung cancer. *Nat Rev Cancer*. 2013;13(4):233–245. doi:10.1038/nrc3477.
- Houghton AM, Mouded M, Shapiro SD. Common origins of lung cancer and COPD. *Nat Med*. 2008;14(10):1023–1024. doi:10.1038/nm1008-1023.
- Vestbo J, Hurd SS, Agustí AG, Jones PW, Vogelmeier C, Anzueto A, Barnes PJ, Fabbri LM, Martinez FJ, Nishimura M, et al. Global strategy for the diagnosis, management, and prevention of chronic obstructive pulmonary disease: GOLD executive summary. *Am J Respir Crit Care Med*. 2013;187(4):347–365. doi:10.1164/rccm.201204-0596PP.
- Young RP, Hopkins RJ, Christmas T, Black PN, Metcalf P, Gamble GD. COPD prevalence is increased in lung cancer, independent of age, sex and smoking history. *Eur Respir J*. 2009;34(2):380–386. doi:10.1183/09031936.00144208.
- Hanahan D, Weinberg RA. Hallmarks of cancer: the next generation. *Cell*. 2011;144(5):646–674. doi:10.1016/j.cell.2011.02.013.
- Coussens LM, Pollard JW. Leukocytes in mammary development and cancer. *Cold Spring Harb Perspect Biol*. 2011;3(3). doi:10.1101/cshperspect.a003285.
- Floor SL, Dumont JE, Maenhaut C, Raspe E. Hallmarks of cancer: of all cancer cells, all the time? *Trends Mol Med*. 2012;18(9):509–515. doi:10.1016/j.molmed.2012.06.005.
- Swamy M, Jamora C, Havran W, Hayday A. Epithelial decision makers: in search of the ‘epimmunome’. *Nat Immunol*. 2010;11(8):656–665. doi:10.1038/ni.1905.
- Blair RJ, Meng H, Marchese MJ, Ren S, Schwartz LB, Tonnesen MG, Gruber BL. Human mast cells stimulate vascular tube formation. Tryptase is a novel, potent angiogenic factor. *J Clin Invest*. 1997;99(11):2691–2700. doi:10.1172/JCI119458.
- Chen R, Ning G, Zhao ML, Fleming MG, Diaz LA, Werb Z, Liu Z. Mast cells play a key role in neutrophil recruitment in experimental bullous pemphigoid. *J Clin Invest*. 2001;108(8):1151–1158. doi:10.1172/JCI11494.
- Galli SJ, Kalesnikoff J, Grimbaldeston MA, Piliponsky AM, Williams CM, Tsai M. Mast cells as “tunable” effector and

- immunoregulatory cells: recent advances. *Annu Rev Immunol.* 2005;23:749–23786. doi:10.1146/annurev.immunol.21.120601.141025.
15. Theoharides TC, Kempuraj D, Tagen M, Conti P, Kalogeromitros D. Differential release of mast cell mediators and the pathogenesis of inflammation. *Immunol Rev.* 2007;217:65–21778. doi:10.1111/j.1600-065X.2007.00519.x.
 16. Galli SJ, Nakae S, Tsai M. Mast cells in the development of adaptive immune responses. *Nat Immunol.* 2005;6(2):135–142. doi:10.1038/ni1158.
 17. Kitamura Y. Heterogeneity of mast cells and phenotypic change between subpopulations. *Annu Rev Immunol.* 1989;7:59–776. doi:10.1146/annurev.iv.07.040189.000423.
 18. Marone G, Triggiani M, Genovese A, De Paulis A. Role of human mast cells and basophils in bronchial asthma. *Adv Immunol.* 2005;88:97–160. doi:10.1016/S0065-2776(05)88004-6.
 19. Metcalfe DD, Baram D, Mekori YA. Mast cells. *Physiol Rev.* 1997;77(4):1033–1079. doi:10.1152/physrev.1997.77.4.1033.
 20. Dalton DK, Noelle RJ. The roles of mast cells in anticancer immunity. *Cancer Immunol Immunother.* 2012;61(9):1511–1520. doi:10.1007/s00262-012-1246-0.
 21. Pittoni P, Colombo MP. The dark side of mast cell-targeted therapy in prostate cancer. *Cancer Res.* 2012;72(4):831–835. doi:10.1158/0008-5472.CAN-11-3110.
 22. Sinnamon MJ, Carter KJ, Sims LP, Lafleur B, Fingleton B, Mattrisian LM. A protective role of mast cells in intestinal tumorigenesis. *Carcinogenesis.* 2008;29(4):880–886. doi:10.1093/carcin/bgn040.
 23. Soucek L, Lawlor ER, Soto D, Shchors K, Swigart LB, Evan GI. Mast cells are required for angiogenesis and macroscopic expansion of Myc-induced pancreatic islet tumors. *Nat Med.* 2007;13(10):1211–1218. doi:10.1038/nm1649.
 24. Theoharides TC. Mast cells and pancreatic cancer. *New Eng J Med.* 2008;358(17):1860–1861. doi:10.1056/NEJMcibr0801519.
 25. Varricchi G, Galdiero MR, Loffredo S, Marone G, Iannone R, Marone G, Granata F. Are mast cells MASTers in cancer? *Front Immunol.* 2017;8:424. doi:10.3389/fimmu.2017.00424.
 26. Dudeck A, Dudeck J, Scholten J, Petzold A, Surianarayanan S, Kohler A, Peschke K, Vohringer D, Waskow C, Krieg T, et al. Mast cells are key promoters of contact allergy that mediate the adjuvant effects of haptens. *Immunity.* 2011;34(6):973–984. doi:10.1016/j.immuni.2011.03.028.
 27. Feyerabend TB, Weiser A, Tietz A, Stassen M, Harris N, Kopf M, Radermacher P, Moller P, Benoist C, Mathis D, et al. Cre-mediated cell ablation contests mast cell contribution in models of antibody- and T cell-mediated autoimmunity. *Immunity.* 2011;35(5):832–844. doi:10.1016/j.immuni.2011.09.015.
 28. Imada A, Shijubo N, Kojima H, Abe S. Mast cells correlate with angiogenesis and poor outcome in stage I lung adenocarcinoma. *Eur Respir J.* 2000;15(6):1087–1093. PMID:10885428.
 29. Redente EF, Orlicky DJ, Bouchard RJ, Malkinson AM. Tumor signaling to the bone marrow changes the phenotype of monocytes and pulmonary macrophages during urethane-induced primary lung tumorigenesis in A/J mice. *Am J Pathol.* 2007;170(2):693–708. doi:10.2353/ajpath.2007.060566.
 30. Stoyanov E, Uddin M, Mankuta D, Dubinett SM, Levi-Schaffer F. Mast cells and histamine enhance the proliferation of non-small cell lung cancer cells. *Lung Cancer.* 2012;75(1):38–44. doi:10.1016/j.lungcan.2011.05.029.
 31. Xiao H, Lasser C, Shelke GV, Wang J, Radinger M, Lunavat TR, Malmhall C, Lin LH, Li J, Li L, et al. Mast cell exosomes promote lung adenocarcinoma cell proliferation - role of KIT-stem cell factor signaling. *Cell Commun Signal.* 2014;12:64. doi:10.1186/s12964-014-0064-8.
 32. Agalioti T, Giannou AD, Krontira AC, Kanellakis NI, Kati D, Vreka M, Pepe M, Spella M, Lilis I, Zazara DE, et al. Mutant KRAS promotes malignant pleural effusion formation. *Nat Commun.* 2017;8:15205. doi:10.1038/ncomms15205.
 33. Giannou AD, Marazioti A, Spella M, Kanellakis NI, Apostolopoulou H, Psalidas I, Prijovich ZM, Vreka M, Zazara DE, Lilis I, et al. Mast cells mediate malignant pleural effusion formation. *J Clin Invest.* 2015;125(6):2317–2334. doi:10.1172/JCI79840.
 34. Marazioti A, Lilis I, Vreka M, Apostolopoulou H, Kalogeropoulou A, Giopanou I, Giotopoulou GA, Krontira AC, Iliopoulou M, Kanellakis NI, et al. Myeloid-derived interleukin-1beta drives oncogenic KRAS-NF-kappaB addition in malignant pleural effusion. *Nat Commun.* 2018;9(1):672. doi:10.1038/s41467-018-03051-z.
 35. Nikitin AY, Alcaraz A, Anver MR, Bronson RT, Cardiff RD, Dixon D, Fraire AE, Gabrielson EW, Gunning WT, Haines DC, et al. Classification of proliferative pulmonary lesions of the mouse: recommendations of the mouse models of human cancers consortium. *Cancer Res.* 2004;64(7):2307–2316. doi:10.1158/0008-5472.CAN-03-3376.
 36. Spella M, Vreka M, Marazioti A, Giopanou I, Aidinis V, Stathopoulos GT. An airway epithelial origin for tobacco carcinogen-induced lung adenocarcinoma. *Eur Respir J.* 2015;46:OA4980. doi:10.1183/13993003.congress-2015.OA4980.
 37. Stathopoulos GT, Sherrill TP, Cheng DS, Scoggins RM, Han W, Polosukhin VV, Connelly L, Yull FE, Fingleton B, Blackwell TS. Epithelial NF-kappaB activation promotes urethane-induced lung carcinogenesis. *Proc Natl Acad Sci U S A.* 2007;104(47):18514–18519. doi:10.1073/pnas.0705316104.
 38. Westcott PM, Halliwilli KD, To MD, Rashid M, Rust AG, Keane TM, Delrosario R, Jen KY, Gurley KE, Kemp CJ, et al. The mutational landscapes of genetic and chemical models of Kras-driven lung cancer. *Nature.* 2015;517(7535):489–492. doi:10.1038/nature13898.
 39. Desai TJ, Brownfield DG, Krasnow MA. Alveolar progenitor and stem cells in lung development, renewal and cancer. *Nature.* 2014;507(7491):190–194. doi:10.1038/nature12930.
 40. Jackson EL, Willis N, Mercer K, Bronson RT, Crowley D, Montoya R, Jacks T, Tuveson DA. Analysis of lung tumor initiation and progression using conditional expression of oncogenic K-ras. *Genes Dev.* 2001;15(24):3243–3248. doi:10.1101/gad.943001.
 41. Giannou AD, Marazioti A, Kanellakis NI, Giopanou I, Lilis I, Zazara DE, Ntaliarda G, Kati D, Armenis V, Giotopoulou GA, et al. NRAS destines tumor cells to the lungs. *EMBO Mol Med.* 2017;9(5):672–686. doi:10.15252/emmm.201606978.
 42. Giopanou I, Lilis I, Papaleonidopoulos V, Agalioti T, Kanellakis NI, Spiropoulou N, Spella M, Stathopoulos GT. Tumor-derived osteopontin isoforms cooperate with TRP53 and CCL2 to promote lung metastasis. *Oncoimmunology.* 2017;6(1):e1256528. doi:10.1080/2162402X.2016.1256528.
 43. Stathopoulos GT, Sherrill TP, Karabela SP, Goleniewska K, Kalomenidis I, Roussos C, Fingleton B, Yull FE, Peebles RS Jr., Blackwell TS. Host-derived interleukin-5 promotes adenocarcinoma-induced malignant pleural effusion. *Am J Respir Crit Care Med.* 2010;182(10):1273–1281. doi:10.1164/rccm.201001-0001OC.
 44. Tono T, Tsujimura T, Koshimizu U, Kasugai T, Adachi S, Isozaki K, Nishikawa S, Morimoto M, Nishimune Y, Nomura S, et al. c-kit Gene was not transcribed in cultured mast cells of mast cell-deficient Wsh/Wsh mice that have a normal number of erythrocytes and a normal c-kit coding region. *Blood.* 1992;80(6):1448–1453. PMID:1381627.
 45. Clausen BE, Burkhardt C, Reith W, Renkawitz R, Forster I. Conditional gene targeting in macrophages and granulocytes using LysMcre mice. *Transgenic Res.* 1999;8(4):265–277. doi:10.1023/A:1008942828960.
 46. Thornberry NA, Bull HG, Calaycay JR, Chapman KT, Howard AD, Kostura MJ, Miller DK, Molineaux SM, Weidner JR, Aunins J, et al. A novel heterodimeric cysteine protease is required for interleukin-1 beta processing in monocytes. *Nature.* 1992;356(6372):768–774. doi:10.1038/356768a0.
 47. Michel A, Schuler A, Friedrich P, Doner F, Bopp T, Radsak M, Hoffmann M, Relle M, Distler U, Kuharev J, et al. Mast cell-deficient Kit(W-sh) “Sash” mutant mice display aberrant myelopoiesis leading to the accumulation of splenocytes that act as

- myeloid-derived suppressor cells. *J Immunol.* 2013;190(11):5534–5544. doi:10.4049/jimmunol.1203355.
48. Horai R, Asano M, Sudo K, Kanuka H, Suzuki M, Nishihara M, Takahashi M, Iwakura Y. Production of mice deficient in genes for interleukin (IL)-1alpha, IL-1beta, IL-1alpha/beta, and IL-1 receptor antagonist shows that IL-1beta is crucial in turpentine-induced fever development and glucocorticoid secretion. *J Exp Med.* 1998;187(9):1463–1475. doi:10.1084/jem.187.9.1463.
 49. Boring L, Gosling J, Chensue SW, Kunkel SL, Farese RV Jr., Broxmeyer HE, Charo IF. Impaired monocyte migration and reduced type 1 (Th1) cytokine responses in C-C chemokine receptor 2 knockout mice. *J Clin Invest.* 1997;100(10):2552–2561. doi:10.1172/JCI119798.
 50. Giopanou I, Lilis I, Papaleonidopoulos V, Marazioti A, Spella M, Vreka M, Papadaki H, Stathopoulos GT. Comprehensive evaluation of nuclear factor-kappaBeta expression patterns in non-small cell lung cancer. *PLoS One.* 2015;10(7):e0132527. doi:10.1371/journal.pone.0132527.
 51. Kasprzyk A. BioMart: driving a paradigm change in biological data management. *Database (Oxford).* 2011;2011bar049. doi:10.1093/database/bar049.
 52. Marwitz S, Depner S, Dvornikov D, Merkle R, Szczygiel M, Muller-Decker K, Lucarelli P, Wasch M, Mairbaurl H, Rabe KF, et al. Downregulation of the TGFbeta pseudoreceptor BAMBI in non-small cell lung cancer enhances TGFbeta signaling and invasion. *Cancer Res.* 2016;76(13):3785–3801. doi:10.1158/0008-5472.CAN-15-1326.
 53. Kabbout M, Garcia MM, Fujimoto J, Liu DD, Woods D, Chow CW, Mendoza G, Momin AA, James BP, Solis L, et al. ETS2 mediated tumor suppressive function and MET oncogene inhibition in human non-small cell lung cancer. *Clin Cancer Res.* 2013;19(13):3383–3395. doi:10.1158/1078-0432.CCR-13-0341.
 54. Györfy B, Surowiak P, Budczies J, Lanczky A. Online survival analysis software to assess the prognostic value of biomarkers using transcriptomic data in non-small-cell lung cancer. *PLoS One.* 2013;8(12):e82241. doi:10.1371/journal.pone.0082241.
 55. Blumenschein GR Jr., Saintigny P, Liu S, Kim ES, Tsao AS, Herbst RS, Alden C, Lee JJ, Tang X, Stewart DJ, et al. Comprehensive biomarker analysis and final efficacy results of sorafenib in the BATTLE trial. *Clin Cancer Res.* 2013;19(24):6967–6975. doi:10.1158/1078-0432.CCR-12-1818.
 56. Byers LA, Diao L, Wang J, Saintigny P, Girard L, Peyton M, Shen L, Fan Y, Giri U, Tumula PK, et al. An epithelial-mesenchymal transition gene signature predicts resistance to EGFR and PI3K inhibitors and identifies Axl as a therapeutic target for overcoming EGFR inhibitor resistance. *Clin Cancer Res.* 2013;19(1):279–290. doi:10.1158/1078-0432.CCR-12-1558.
 57. Morita H, Arae K, Unno H, Miyauchi K, Toyama S, Nambu A, Oboki K, Ohno T, Motomura K, Matsuda A, et al. An interleukin-33-mast cell-interleukin-2 axis suppresses papain-induced allergic inflammation by promoting regulatory T cell numbers. *Immunity.* 2015;43(1):175–186. doi:10.1016/j.immuni.2015.06.021.
 58. Zaynagetdinov R, Stathopoulos GT, Sherrill TP, Cheng DS, McLoed AG, Ausborn JA, Polosukhin VV, Connelly L, Zhou W, Fingleton B, et al. Epithelial nuclear factor-kappaB signaling promotes lung carcinogenesis via recruitment of regulatory T lymphocytes. *Oncogene.* 2012;31(26):3164–3176. doi:10.1038/onc.2011.480.
 59. Ridker PM, MacFadyen JG, Thuren T, Everett BM, Libby P, Glynn RJ, Group CT. Effect of interleukin-1beta inhibition with canakinumab on incident lung cancer in patients with atherosclerosis: exploratory results from a randomised, double-blind, placebo-controlled trial. *Lancet.* 2017;390(10105):1833–1842. doi:10.1016/S0140-6736(17)32247-X.
 60. Ridker PM, MacFadyen JG, Everett BM, Libby P, Thuren T, Glynn RJ, Group CT. Relationship of C-reactive protein reduction to cardiovascular event reduction following treatment with canakinumab: a secondary analysis from the CANTOS randomised controlled trial. *Lancet.* 2018;391(10118):319–328. doi:10.1016/S0140-6736(17)32814-3.
 61. Schindelin J, Arganda-Carreras I, Frise E, Kaynig V, Longair M, Pietzsch T, Preibisch S, Rueden C, Saalfeld S, Schmid B, et al. Fiji: an open-source platform for biological-image analysis. *Nat Methods.* 2012;9(7):676–682. doi:10.1038/nmeth.2019.
 62. Hsia CC, Hyde DM, Ochs M, Weibel ER, Structure AEJTFoQAoL. An official research policy statement of the American Thoracic Society/European Respiratory Society: standards for quantitative assessment of lung structure. *Am J Respir Crit Care Med.* 2010;181(4):394–418. doi:10.1164/rccm.200809-1522ST.
 63. Travis WD, Brambilla E, Noguchi M, Nicholson AG, Geisinger KR, Yatabe Y, Beer DG, Powell CA, Riely GJ, Van Schil PE, et al. International association for the study of lung cancer/american thoracic society/european respiratory society international multidisciplinary classification of lung adenocarcinoma. *J Thorac Oncol.* 2011;6(2):244–285. doi:10.1097/JTO.0b013e318206a221.
 64. Pfaffl MW. A new mathematical model for relative quantification in real-time RT-PCR. *Nucleic Acids Res.* 2001;29(9):e45. PMID:11328886. doi:10.1093/nar/29.9.e45.
 65. Subramanian A, Tamayo P, Mootha VK, Mukherjee S, Ebert BL, Gillette MA, Paulovich A, Pomeroy SL, Golub TR, Lander ES, et al. Gene set enrichment analysis: a knowledge-based approach for interpreting genome-wide expression profiles. *Proc Natl Acad Sci U S A.* 2005;102(43):15545–15550. doi:10.1073/pnas.0506580102.
 66. Faul F, Erdfelder E, Lang AG, Buchner A. G*Power 3: a flexible statistical power analysis program for the social, behavioral, and biomedical sciences. *Behav Res Methods.* 2007;39(2):175–191. PMID:17695343.